Cell Reports
Medicine

Article

Adenosine A2A receptor is a tumor suppressor of NASH-associated hepatocellular carcinoma

Graphical abstract

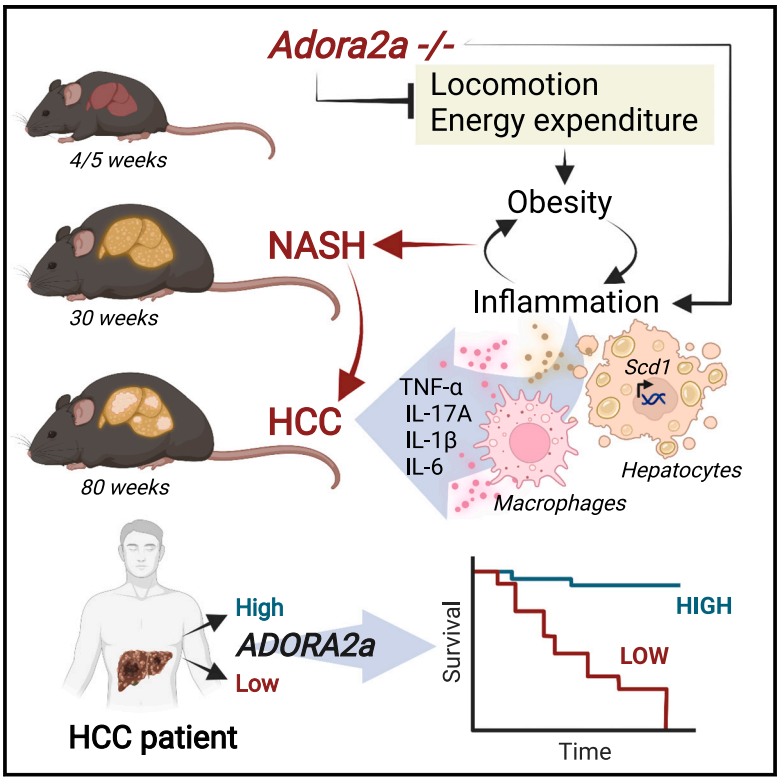

Authors

Bertrand Allard,
Célia Jacoberger-Foissac,
Isabelle Cousineau, ...,
Sebastien Duquenne, Fabien Picard,
John Stagg

Correspondence

john.stagg@umontreal.ca

In brief

Allard et al. uncover a previously unknown role for A2AR in restraining NASH-associated HCC in mice. Myeloid- and hepatocyte-derived A2AR signaling protects liver against HCC development by limiting hepatic inflammation, diet-induced obesity, and steatosis. In patients with HCC, low *ADORA2A* gene expression predicts poor prognosis.

Highlights

- A2AR deficiency triggers spontaneous obesity, inflammation, and NASH-HCC in mice
- Myeloid- and hepatocyte-derived A2AR signaling restrains HCC development
- Steatohepatitis impairs the anti-HCC activity of A2AR pharmacological blockade
- Low *ADORA2A* gene expression predicts poor survival in HCC patients

Allard et al., 2023, Cell Reports Medicine *4*, 101188
September 19, 2023
https://doi.org/10.1016/j.xcrm.2023.101188

CellPress

Cell Reports Medicine

CellPress
OPEN ACCESS

Article

Adenosine A2A receptor is a tumor suppressor of NASH-associated hepatocellular carcinoma

Bertrand Allard,[1,2] Célia Jacoberger-Foissac,[1,2] Isabelle Cousineau,[1,2] Yacine Bareche,[1,2] Laurence Buisseret,[3] Pavel Chrobak,[1,2] David Allard,[1,2] Sandra Pommey,[1,2] Franck Ah-Pine,[4] Sebastien Duquenne,[4] Fabien Picard,[5,6] and John Stagg[1,2,7,*]

[1]Centre de Recherche du Centre Hospitalier de l'Université de Montréal et Institut du Cancer de Montréal, Montreal, QC, Canada
[2]Faculté de Pharmacie, Université de Montréal, Montreal, QC, Canada
[3]Institut Jules Bordet, Bruxelles, Belgium
[4]Department of Pathology, CHU Sud Réunion, Saint-Pierre, France
[5]Montréal Heart Institute, Cardiology Department, Université de Montréal, Montreal, QC, Canada
[6]Hopital Cochin, Cardiology Department, Université de Paris, Paris, France
[7]Lead contact
*Correspondence: john.stagg@umontreal.ca
https://doi.org/10.1016/j.xcrm.2023.101188

SUMMARY

Inhibition of adenosine A2A receptor (A2AR) is a promising approach for cancer immunotherapy currently evaluated in several clinical trials. We here report that anti-obesogenic and anti-inflammatory functions of A2AR, however, significantly restrain hepatocellular carcinoma (HCC) development. Adora2a deletion in mice triggers obesity, non-alcoholic steatohepatitis (NASH), and systemic inflammation, leading to spontaneous HCC and promoting dimethylbenzyl-anthracene (DMBA)- or diethylnitrosamine (DEN)-induced HCC. Conditional Adora2a deletion reveals critical roles of myeloid and hepatocyte-derived A2AR signaling in restraining HCC by limiting hepatic inflammation and steatosis. Remarkably, the impact of A2AR pharmacological blockade on HCC development is dependent on pre-existing NASH. In support of our animal studies, low ADORA2A gene expression in human HCC is associated with cirrhosis, hepatic inflammation, and poor survival. Together, our study uncovers a previously unappreciated tumor-suppressive function for A2AR in the liver and suggests caution in the use of A2AR antagonists in patients with NASH and NASH-associated HCC.

INTRODUCTION

Extracellular adenosine (eADO) is a multifunctional metabolite involved in various pathophysiological conditions.[1,2] eADO accumulates from the breakdown of eATP by membrane-bound ecto-nucleotidases, predominantly CD39 and CD73. Once released in the interstitial space, eADO exerts its biological functions through the local stimulation of P1 purinergic G protein-coupled receptors (GPCRs), namely A1, A2A, A2B, and A3 receptors. Signaling through A2A receptors (A2ARs) notably inhibits local and systemic inflammation and promotes tissue repair.[3]

In the inflamed and hypoxic tumor microenvironment (TME), A2AR-driven immunosuppression promotes tumor development.[4–7] Accordingly, inhibition of A2AR has been shown to delay tumor growth and to promote anti-tumor immunity.[4–6,8–13,13–16] In preclinical cancer models, A2AR blockade enhances the efficacy of various immunotherapies, including immune checkpoint inhibitors, cancer vaccines, and adoptive T cell therapy.[4–6,8–16] In phase 1 clinical trials, A2AR antagonists have been associated with encouraging results, and confirmed clinical responses were reported in various cancer indications.[17,18]

Recent studies highlighted the importance of A2AR signaling in protection against liver damage and inflammation.[19–26] In particular, A2AR expression on immune cells was shown to be critical to protect the liver against various type of injuries involving excessive inflammatory reactions, as encountered during ischemia-reperfusion,[23,25] sepsis, and non-alcoholic steatohepatitis (NASH).[19–22] For this later, hepatocyte-derived A2AR signaling was also evidenced to play a protective role by limiting fatty-acid-induced toxicity, fat deposition, and pro-inflammatory cytokine secretion.[19–22] Accordingly, pharmacological activation of A2AR suppresses,[21,22] while A2AR gene deletion promotes, non-alcoholic fatty liver disease (NAFLD) and NASH in murine models.[19,20] Whether A2AR signaling further impacts the development of NAFLD-/NASH-associated liver cancer remains unknown.

In this study, we demonstrate that silencing of the A2AR gene (*Adora2a*) induces a systemic metabolic dysregulation in mice that triggers the spontaneous development of hepatocellular carcinoma (HCC) and accelerates carcinogen-induced HCC. Bone marrow transplantation and conditional *Adora2a* deletion highlight a prominent role for myeloid- and hepatocyte-derived A2ARs in the suppression of liver carcinogenesis by restraining

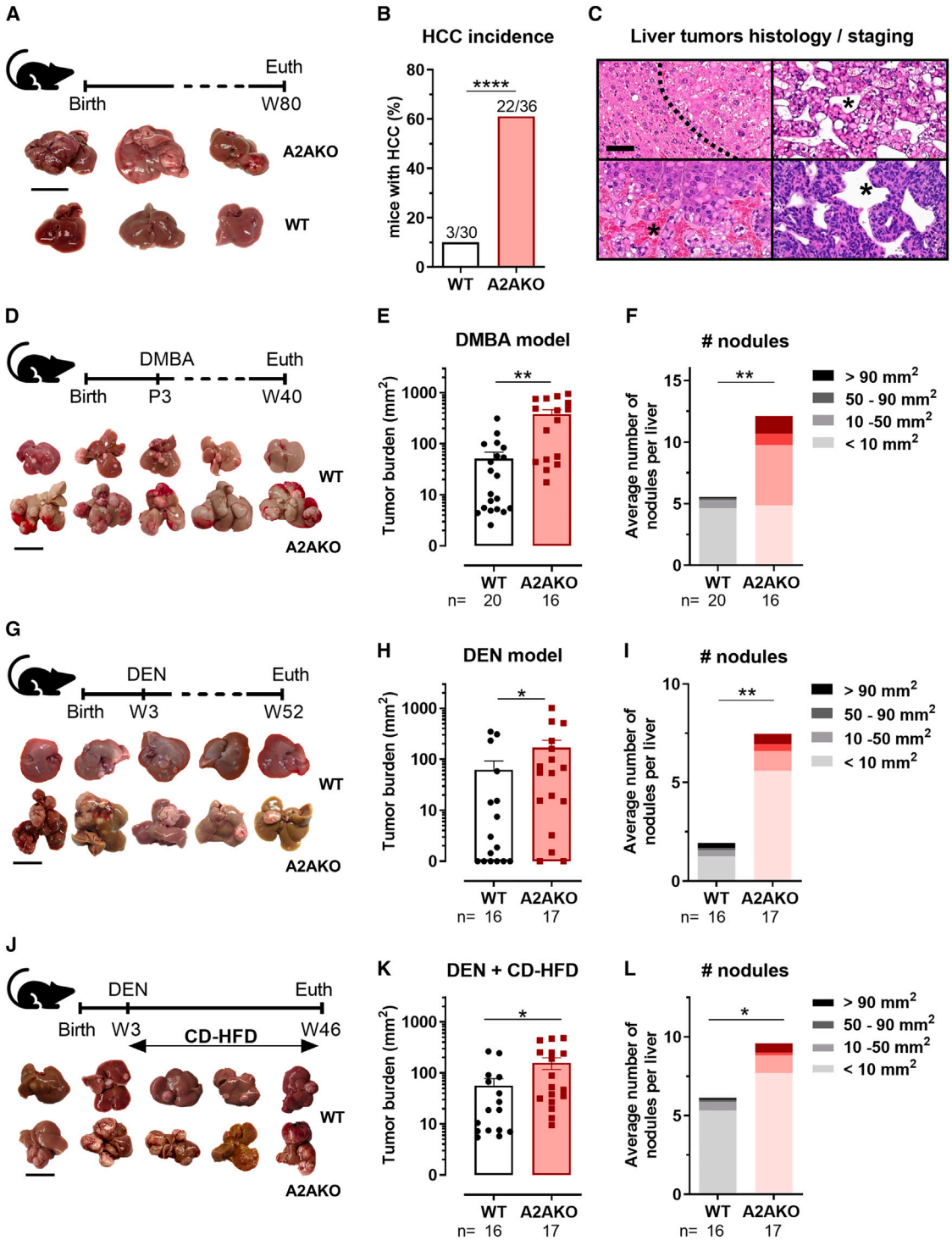

Figure 1. Development of spontaneous and carcinogen-induced HCC is enhanced in A2AR-deficient mice

(A) Experimental setting: WT and A2AR-deficient males were aged to 80 weeks old. Representative pictures of spontaneous HCC observed in WT and A2AR-deficient males are shown. Scale bar represents 2 cm.

(B) HCC incidence (observation of macroscopic lesions) in 80-week-old WT and A2AKO males.

(C) Hematoxylin and eosin staining of cancerous livers collected from A2AKO mice depicting the different stages of HCC: top panel, stages 1 and 2, and bottom panel, stages 3 and 4; scale bar represents 50 μm. An asterisk (*) indicates trabeculae that are present in stage II–IV mouse liver tumors.

(D) Experimental setting: WT and A2AR-deficient pups were treated with DMBA, 3 to 4 days after birth, and aged until 40 weeks old.

(legend continued on next page)

hepatic inflammation and lipogenesis, respectively. Pharmacological experiments reveal that pre-existing NASH impairs the anti-HCC activity of A2AR blockade and that A2AR signaling inhibition in NASH mice exacerbates obesity and myeloid-derived liver inflammation. In human HCC, *ADORA2A* expression levels are inversely correlated with patients' overall survival and with the presence of hepatic inflammation and cirrhosis. Overall, our study uncovers a previously unknown tumor suppressive role of A2AR signaling in liver cancer with potential implications for the clinical use of A2AR antagonists in patients with NASH-HCC.

RESULTS

Global A2AR deletion promotes the development of spontaneous and carcinogen-induced HCC in mice

Necropsy of aged 80-week-old male mice with global A2AR deficiency revealed that 60% of mice (22/36) had spontaneously developed liver cancer. In contrast, only 10% (3/30) of age-matched control mice displayed macroscopic liver lesions (Figures 1A–1C and S1A–C). Pathological analysis confirmed HCC histology, mainly of stages I/II, with few cases of stages III and IV HCC characterized by larger trabeculae and the presence of hemorrhagic and necrotic areas (Figure 1C). Most tumors presented steatosis, hepatocyte degeneration, and inflammatory cell foci, as well as substantial fibrosis, indicating that liver carcinogenesis occurring in A2AR-deficient mice shares many characteristics of NASH-driven HCC in humans (Figures S1D and S1E).

To further evaluate the role of A2AR in liver carcinogenesis, we next used established experimental models of carcinogen-induced HCC involving the administration of dimethylbenzylanthracene (DMBA) or diethylnitrosamine (DEN), including in combination with choline-deficient high-fat diet (CD-HFD) or carbon tetrachloride (CCl_4). As shown in Figures 1D–1L, global A2AR deficiency was associated with a significant increase in HCC tumor burden after DMBA or DEN administration. When DEN was administered with CCl_4 to stimulate chronic liver inflammation, however, the increased susceptibility of A2AR-deficient mice was less pronounced (Figure S2A–S2C). In wild-type (WT) cancerous livers, immunofluorescent staining revealed that A2AR was mainly expressed on hepatocytes and on macrophages (Figures S2F and S2G). In addition, A2AR expression was reduced in tumor nodules as compared to adjacent tissue.

Loss of A2AR signaling triggers spontaneous obesity, NASH, and systemic inflammation

We observed that spontaneous HCC development in aged A2AR-deficient mice was preceded by a significant weight gain and fat tissue accumulation (Figures 2A–2C). Notably, obesity was more pronounced in A2AR-deficient males compared with females and was mitigated in heterozygous ($A2AR^{+/-}$) animals (Figures 2A, S3A, and S3B). At 32 weeks of age, A2AR-deficient mice displayed a significantly greater accumulation of subcutaneous and visceral fat compared with WT controls (Figures 2B and 2C). Fat pads of A2AR-deficient mice showed adipocyte hypertrophy but similar adipocyte density (Figures S3C–S3F), thus excluding an impact of A2AR signaling on adipocyte accumulation. Moreover, food intake was unchanged between WT and A2AR-deficient mice (Figures S3G and S3H), thus ruling out an impact of A2AR signaling on appetite.

Several reports indicate a central role of A2AR signaling in energy homeostasis, notably through the regulation of brown adipose tissue thermogenesis.[27] To better understand what triggers spontaneous obesity in A2AR-deficient mice, we used metabolic cages to compare energy expenditure of young WT and A2AR-deficient mice with similar weights and body compositions. We observed that energy expenditure (EE) was reduced in A2AR-deficient mice as compared with WT mice (Figure S4A–S4C). We also observed a sharp decrease in locomotory activity in A2AR-deficient mice (Figures S4D and S4F), suggesting that impaired locomotion might be responsible for a reduced EE, which, in the long term, could promote the development of obesity.

Obesity is frequently associated with the development of NAFLD and NASH, which constitute strong risk factors for the development of HCC.[28] Livers of A2AR-deficient mice displayed severe steatosis (Figures 2D and 2E), and histopathological analysis revealed typical features of NAFLD and NASH, such as the presence of ballooning hepatocytes, macrovesicular steatosis, and lobular inflammation (Figure 2E). Using a NASH severity score (i.e., NASH scale, or NAS, ranging from 0 to 8), we observed that A2AR-deficient mice displayed a significantly higher NAS compared with WT mice (5.8 versus 1; $p < 0.01$; Figure 2F).

We next compared the mRNA expression levels of pro-inflammatory cytokines in the livers of WT and A2AR-deficient mice. As shown in Figure 2G, the expression of several pro-inflammatory cytokines was significantly increased in A2AR-deficient livers as compared with WT livers. Notably, myeloid-attracting chemokines (e.g., *Ccl2*, *Ccl3*, *Ccl4*, and *Cxcl2*) were particularly augmented in A2AR-deficient livers, as were pro-inflammatory cytokines with a major role in the development of HCC, such as *Il1b*, *Il6*, *Il17a*, and *Tnfa*. Consistent with this observation and with the development of NASH in aged A2AR-deficient mice, we detected an increased expression of macrophage genes (e.g., *Adgre*, *Mrc1*, *Vsig4*), fibrosis genes (e.g., *Col1a1*,

(E and F) Liver tumor burden (total tumor area and nodule number) in 40-week-old mice.
(G) Experimental setting: WT and A2AR-deficient males were treated with DEN (intraperitoneal [i.p.] 50 mg/kg) at 3 weeks old and aged until 52 weeks old.
(H and I) Liver tumor burden (total tumor area and nodule number) in 52-week-old mice.
(J) Experimental setting: WT and A2AR-deficient males were treated with DEN (i.p. 50 mg/kg) at 3 weeks old and fed with CD-HFD until 46 weeks old.
(K and L) Liver tumor burden (total tumor area and nodule number) in 46-week-old mice.
For each experiment, representative pictures of cancerous livers observed in WT and A2AR-deficient males are shown. Results are representative of 1 biological replicate for each HCC model, and sample size is indicated for each panel. Data are presented as means ± SEM. Statistical tests: Mann-Whitney except for (B) (chi-squared test).

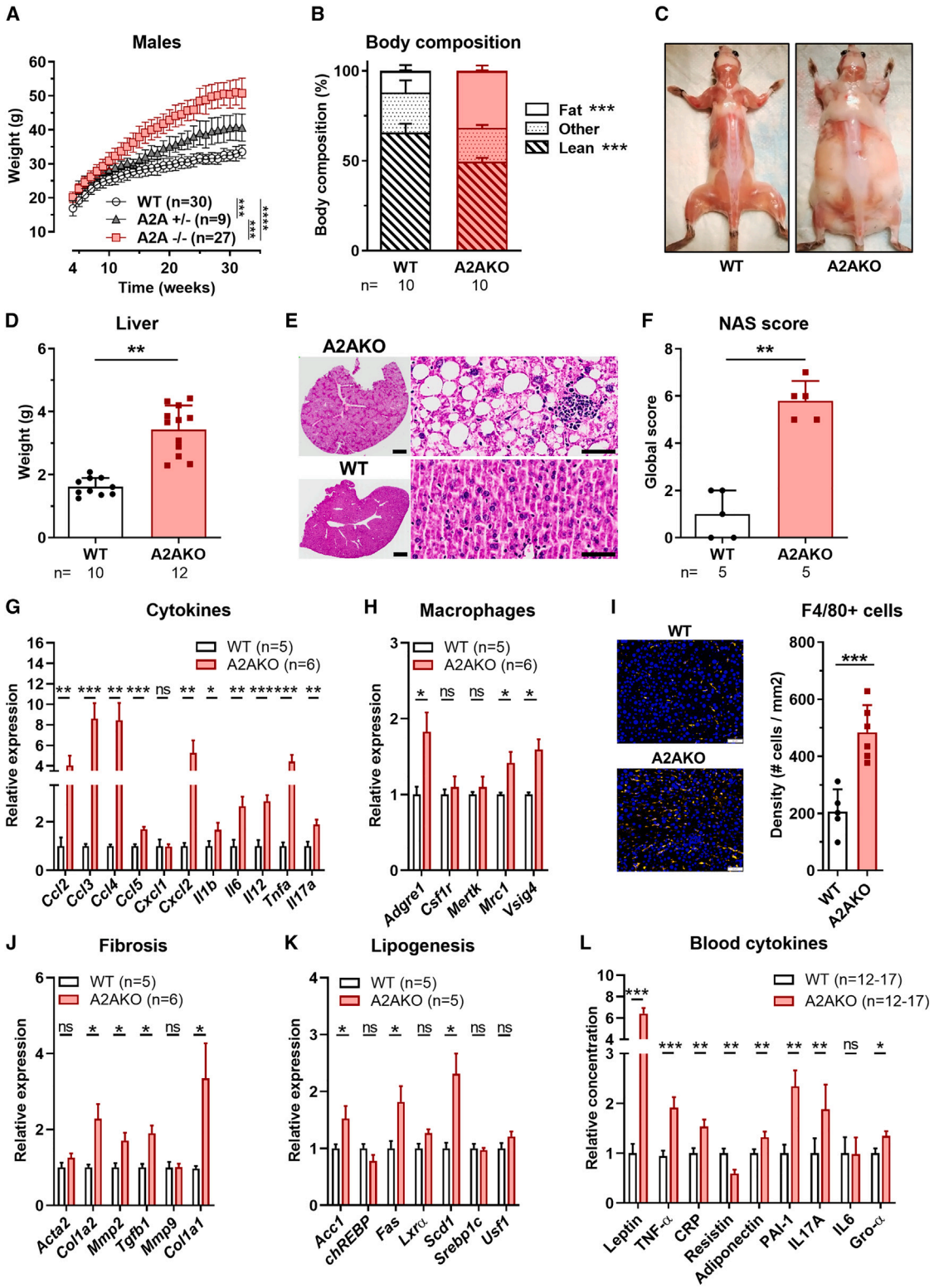

Figure 2. Loss of A2AR signaling triggers spontaneous obesity, NASH, and systemic inflammation

(A) Weight gain of WT, *A2A*$^{-/-}$, and *A2A*$^{+/-}$ mice (males) was monitored weekly starting from week 4 to 32 weeks old.

(B) Body composition of 24-week-old WT and A2AKO males.

(C) Representative picture of 32-week-old WT and A2AKO mice showing fat accumulation in A2AKO animals.

(legend continued on next page)

Col1a2, *Tgfb1*), and lipogenesis markers (e.g., *Acc1*, *Fas*, *Scd1*) in A2AR-deficient livers (Figures 2H–2J). While *Acc1*, *Fas*, and *Scd1* were also upregulated in the liver of young (not yet obese) A2AR animals relative to WT animals, the mRNA levels of other markers were similar in WT and A2AR-deficient livers collected from young animals (Figures S5A–S5D).

Systemic low-grade inflammation and insulin resistance are comorbidities frequently associated with obesity in humans. Consistent with this observation, obese A2AR-deficient mice showed elevated blood concentrations of various pro-inflammatory cytokines and adipokines (Figure 2K), including tumor necrosis factor α (TNF-α), plasminogen activator inhibitor-1 (PAI-1), C-reactive protein (CRP), and leptin, that are commonly increased in humans presenting metabolic syndrome.[29] Interestingly, young A2AR-deficient animals, not yet showing signs of obesity, did not present elevated blood level of these pro-inflammatory markers (Figure S5E). Increased weight gain in A2AR-deficient mice was also associated with impaired blood glucose homeostasis despite elevated blood insulin levels as compared with WT mice, thus suggesting insulin resistance (Figures S5F–S5H).

Myeloid- and hepatocyte-specific deletion of A2AR signaling promotes DMBA-induced HCC development

We next tested the hypothesis that a loss of immune cell-derived A2AR signaling may promote the development of obesity and liver carcinogenesis. In agreement with our hypothesis, transplantation of WT bone marrow into A2AR-deficient mice (Figure S6) significantly reduced both weight gain and the development of DMBA-induced liver cancer compared with mice with complete A2AR deficiency (Figures S6A–S6E). Grafting A2AR-deficient bone marrow into WT mice (A2A into WT), however, was not sufficient to promote weight gain or to exacerbate liver carcinogenesis. Interestingly, when mice were fed with HFD, hematopoietic-specific deficiency in A2AR was sufficient to promote weight gain and increase fat mass in chimeric mice (Figures S6F and S6G).

A2AR signaling in macrophages and hepatocytes was shown to act in concert to restrain HFD-induced liver inflammation and steatosis-causing NAFLD.[19] We thus generated mice with myeloid-specific ($A2AR^{fl/fl}$ *LysM-Cre*$^{+/-}$) or hepatocyte-specific ($A2AR^{fl/fl}$ AAV8-TBG-Cre) deletion of A2AR (Figures 3I and 3J) and evaluated the impact on the development of HFD-induced obesity and DMBA-induced liver cancer (Figure 3A). While myeloid-specific deletion of A2AR had no impact on weight gain, hepatocyte-specific A2AR deficiency accelerated HFD-induced obesity relative to control mice (Figure 3C). Interestingly, both myeloid- and hepatocyte-specific A2AR deficiency enhanced the development of DMBA-induced HCC as compared with control mice (Figures 3B, 3D, and 3E). Myeloid-specific deficiency, but not hepatocyte-specific deficiency, in A2AR signaling enhanced the mRNA levels of various pro-inflammatory and pro-tumorigenic cytokines in the liver (Figure 3F). In contrast, mRNA levels of lipogenesis markers remained globally unchanged upon myeloid- or hepatocyte-specific A2AR silencing, except for *Scd1*, which was significantly decreased in myeloid-specific A2AR-deficient mice and upregulated in hepatocyte-specific A2AR-deficient mice (Figure 3G). Finally, we observed an increased number of CD11b+ F4/80+ macrophages in the liver of mice lacking A2AR expression in the myeloid compartment and, to a lesser extent, in mice lacking A2AR expression on hepatocytes (Figure 3H).

Increased liver tumorigenesis in A2AR-deficient mice is TNF-α, IL-1β, and IL-17A dependent

We next tested the hypothesis that A2AR signaling was required to restrain the secretion of pro-inflammatory cytokines known to promote HCC development. Using the DMBA-induced liver cancer model, we indeed demonstrated that exacerbated HCC development in A2AR-deficient mice can be reversed by neutralizing TNF-α, interleukin 1β (IL-1β), or IL-17A (Figure 4A). Blocking one of these cytokines significantly reduced liver tumor development in A2AR-deficient mice (Figures 4B and 4D–4F). Of note, neutralizing IL-6 activity showed a trend toward reduced HCC development in A2AR-deficient mice, but this was not statistically significant. Interestingly, none of these cytokines were involved in A2AR-deficiency-induced obesity (Figure 4C).

Pharmacological blockade of A2AR promotes HFD-induced obesity and liver inflammation

To consolidate our observations in A2AR-deficient mice and provide translational relevance to our findings, we tested the impact of pharmacological inhibition of A2AR signaling on the development of HFD-induced obesity, liver inflammation, and liver steatosis. We observed that A2AR blockade with the specific antagonist KW6002 significantly exacerbated HFD-induced obesity, while stimulation of A2AR using the specific agonist CGS28160 prevented weight gain (Figures 5A and 5B). Similar results were obtained using another A2AR antagonist, namely NIR178, currently in clinical trial (Figures S8C and S8D). Using multicolor flow cytometry, we compared the liver immune infiltrate of HFD-fed mice treated with KW6002, CGS28160, or vehicle. Chronic KW6002 administration increased the accumulation of

(D) Liver weights of 32-week-old WT and A2AKO males.
(E) Hematoxylin and eosin (H&E) staining of livers collected from 32-week-old WT and A2AKO males. Scale bars represent 1 mm (left panels) and 100 μm (right panels).
(F) NASH scores of WT and A2AKO livers.
(G, H, J, and K) Real-time PCR showing comparative expression of pro-inflammatory cytokines (G), macrophage markers (H), fibrosis markers (J), and lipogenesis markers (K) in WT and A2AKO livers collected from 32-week-old males.
(I) WT and A2AKO liver sections were stained with anti-F4/80 antibody to evaluate macrophage density. Representative pictures are shown with F4/80 staining in yellow and DAPI counterstain in blue. Scale bar represents 50 μm.
(L) Blood concentration of inflammatory markers in WT and A2AKO mice at 30 weeks of age.
Results are representative of 1 biological replicate, and sample size is indicated for each panel. Data are presented as means ± SEM. Statistical tests: Student's t test or multiple t tests with Benjamin-Hochberg multiple comparison correction.

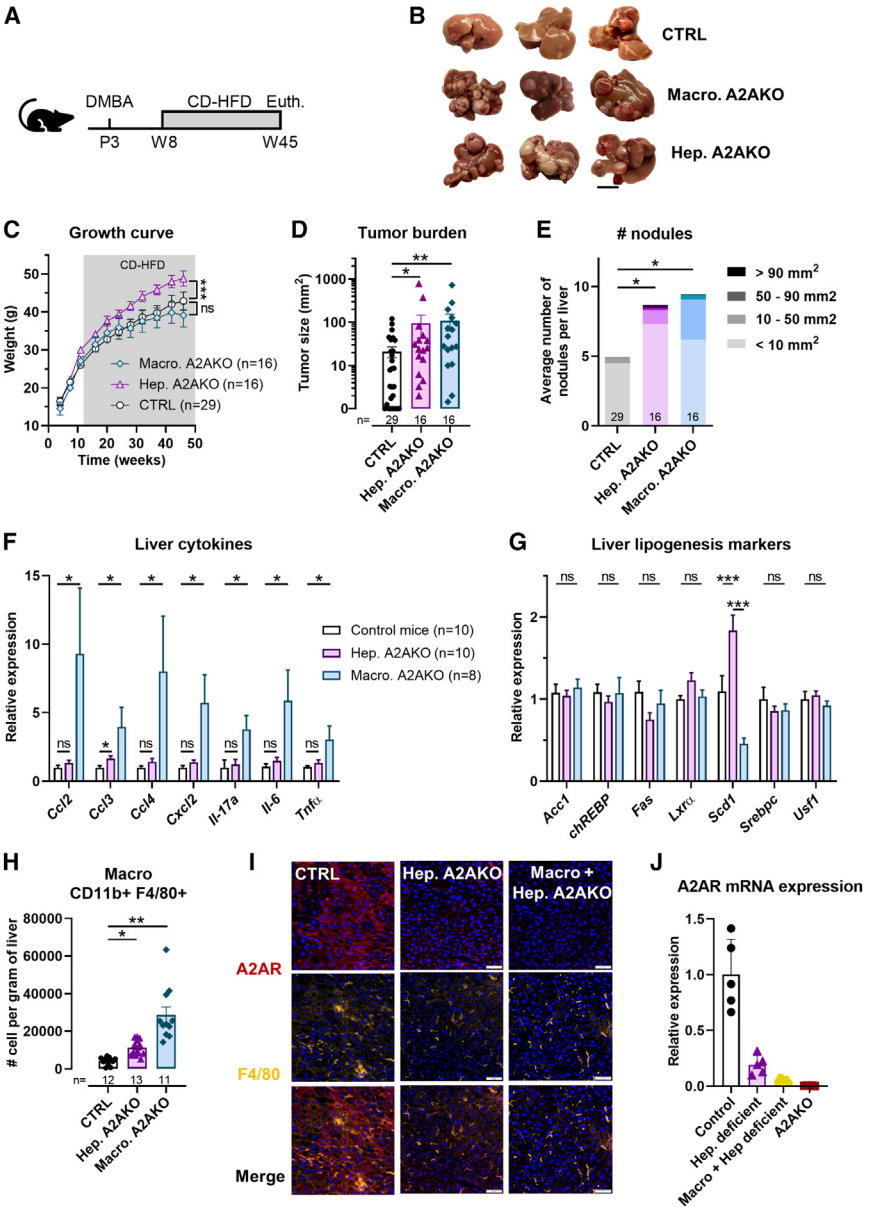

Figure 3. Myeloid- and hepatocyte-specific deletions of A2AR signaling promotes DMBA-induced HCC development

(A) Experimental setting: *lyzM-Cre*$^{+/-}$ A2AR$^{flox/flox}$ pups (myeloid-specific deficiency) or *LyzM-Cre*$^{-/-}$ A2AR$^{flox/flox}$ pups were treated with DMBA and switched to CD-HFD from 8 to 45 weeks old. Some *LyzM-Cre*$^{-/-}$ A2AR$^{flox/flox}$ pups were injected with AAV8-TBG-Cre viruses to generate hepatocyte-specific A2AR-deficient mice.

(B) Representative pictures comparing livers of 42-week-old mice with myeloid-specific or hepatocyte-specific deficiency in A2AR signaling.

(C–E) Growth curve (C), total liver tumor burden (D), and average number of liver nodules (E) of CD-HFD-fed mice with or without myeloid- or hepatocyte-specific deficiency in A2AR signaling.

(F and G) Real-time PCR showing comparative expression of pro-inflammatory cytokines genes (F) or lipogenesis markers (G) in the liver of mice with or without myeloid- or hepatocyte-specific deficiency in A2AR signaling.

(H) Abundance of liver-derived CD11b+ F4/80+ macrophages in mice with myeloid- or hepatocyte-specific deficiency in A2AR signaling was analyzed by flow cytometry.

(I) Formalin-fixed, paraffin-embedded (FFPE) liver sections from A2AR-proficient (control) mice or mice bearing specific A2AR deficiency on hepatocytes (Hep. deficient) or on hepatocyte and macrophage (macro + hep. deficient) were stained for A2AR (top panels) and F4/80 (middle panels). Bottom panels display merged pictures showing A2AR and F4/80 co-staining. Scale bar represents 50 μm.

(J) Measurement of liver A2AR mRNA expression by real-time quantitative PCR (1 biological replicate, n = 5).

Results are representative of 1 biological replicate, and sample size is indicated for each panel. Data are presented as means ± SEM. Statistical tests: Student's t test (C), multiple t tests with Benjamin-Hochberg multiple comparison correction (F–H), or Kruskal-Wallis with Dunn's correction (D and E).

CD11b+ Ly6C^{high} inflammatory monocytes, while CGS28160 showed profound anti-inflammatory activity on various myeloid cell subsets including macrophages, monocytes, and neutrophils (Figures 5E–5L). KW6002 or CGS28160 treatments did not display any significant impact on lymphoid cell infiltrate, except for CD4^{+} T cells, which were significantly diminished upon KW6002 administration (Figure 5J). In line with these observations, KW6002 upregulated the expression of myeloid-attracting chemokines (*Ccl2*, *Ccl3*, *Ccl4*, and *Cxcl2*) in the liver (Figure 5M). In addition, chronic administration of KW6002 significantly upregulated mRNA levels of liver-derived *Tnf-α*, which is a primary HCC-promoting cytokine. In contrast, CGS28160 reduced the mRNA expression of all the pro-inflammatory cytokines/chemokines tested (Figure 5M). mRNA levels of various lipogenic markers were unaffected by the KW6002 or CGS28160 treatment (Figure 5N).

Diet-induced steatohepatitis impairs the anti-HCC activity of A2AR blockade

To evaluate the impact of A2AR signaling blockade on the development of HCC, we used a short-term, transposon-based hydrodynamic tail-vein (HTV) HCC model. HCC development was triggered by the overexpression of a constitutively active form of Akt (myr-Akt) coupled to CRISPR-Cas9-mediated knockdown of TP53 expression in hepatocytes using HTV injections (Figure 6A). Using this model, we observed that the specific A2AR antagonist KW6002 potently delayed HCC development as compared to mice receiving vehicle

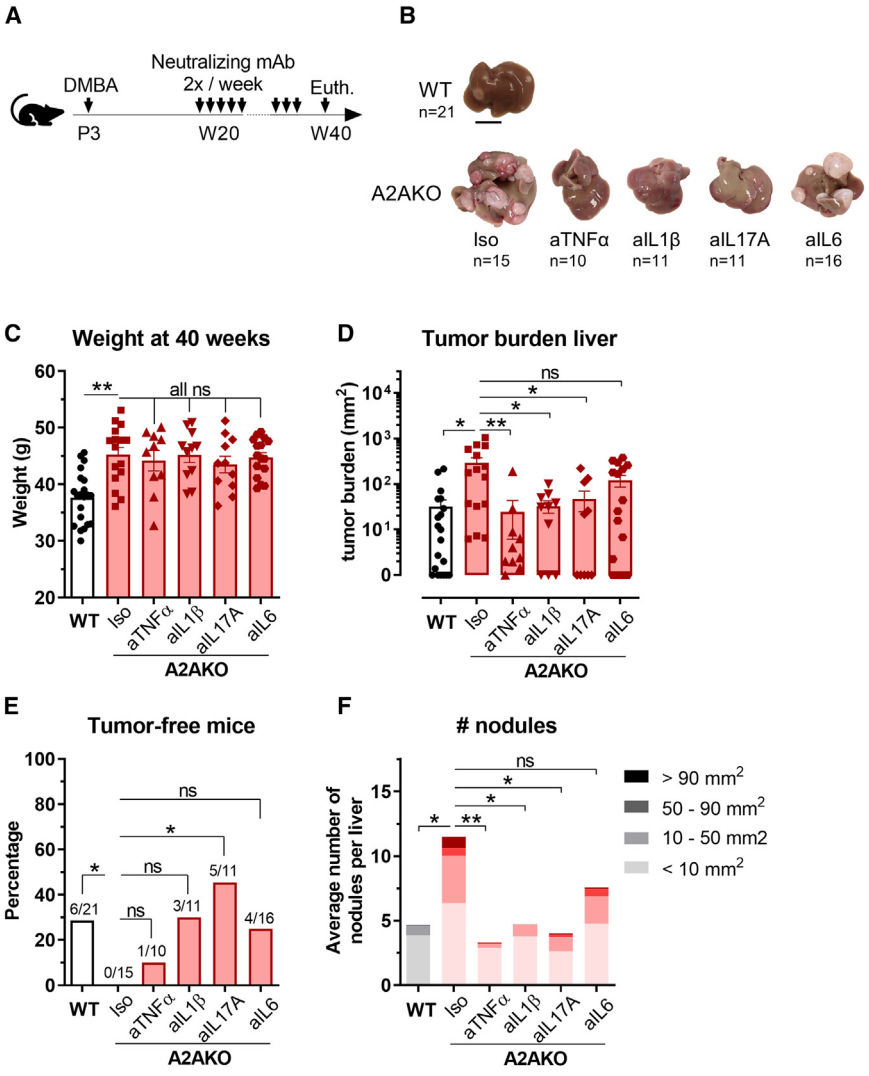

Figure 4. Exacerbated development of HCC in A2AR-deficient mice is TNF-α, IL-1β, and IL-17A dependent

(A) Experimental setting: WT and A2AKO pups were treated with DMBA. At week 20, A2AKO mice were split into 5 groups receiving isotype control antibody or neutralizing monoclonal antibody (mAb) against TNF-α, IL-1β, IL-17A, and IL-6. Mice were sacrificed at 40 weeks old to evaluate tumor burden.

(B) Representative pictures showing livers of 40-week-old A2AR-deficient mice treated with isotype control or anti-cytokine neutralizing mAbs.

(C) Mice weights at 40 weeks old.

(D) Total liver tumor burden.

(E) Tumor incidence.

(F) Number of macroscopic nodules.

Results are representative of 1 biological replicate, and sample size is indicated for each panel. Data are presented as means ± SEM. Statistical tests: multiple t tests with Benjamin-Hochberg multiple comparison correction (C), Kruskal-Wallis with Dunn's correction (D and F), or chi-squared test (E).

(Figures 6B–6E). Most mice treated with KW6002 had no visible macroscopic liver lesions as compared with vehicle-treated animals (10/13 versus 4/13, respectively, $p < 0.05$), and HCC nodules were smaller in KW6002-treated animals. To test the impact of A2AR inhibition on the development of NASH-HCC, mice were fed with a CD-HFD before triggering the development of HCC through HTV injections. In these conditions, A2AR blockade failed to delay liver tumor development as opposed to the results obtained under regular diet feeding (Figures 6C–6E). Similar results were obtained when evaluating the impact of chronic KW6002 treatment on mice exposed to DMBA and fed with a CD-HFD (Figures 6F–6I). Together, our results indicate that steatohepatitis impairs the anti-tumor activity of A2AR blockade against liver tumors.

Reduced ADORA2A expression predicts poor prognosis in patients with HCC

We next investigated the prognostic impact of *ADORA2A* gene expression in human patients with HCC. Using the UCSC Xena functional genomic explorer, we first compared *ADORA2A* expression in tumoral versus healthy liver tissues. We observed a significant reduction of *ADORA2A* expression level in HCC compared with healthy liver biospecimens (Figure 7A). We then correlated *ADORA2A* expression with overall survival (OS) in HCC patient cohorts. In a meta-analysis incorporating 4 different cohorts (which totals nearly 900 patients with HCC), reduced *ADORA2A* expression was significantly associated with a worse OS (Figures 7B, 7C, and S7). After correction for potentially confounding factors relevant for prognosis, such as tumor stage, tumor grade, or ethnicity, reduced *ADORA2A* expression remained independently associated with shorter OS in the TCGA HCC cohort (hazard ratio [HR] 0.59; 95% confidence interval [CI] 0.38–0.91; $p = 0.016$; Table S1). We also observed that reduced *ADORA2A* expression was predictive of worse OS in both viral and alcohol-related HCC but not in patients with HCC with no history of primary risk factors (Figures 7D–7F). The paucity of patients with NAFLD-/NASH-related HCC prevented the analysis of ADORA2A prognostic value for this subgroup. Using the publicly available diagnosis slides of the TCGA LIHC cohort, we then explored the association of *ADORA2A* expression with histological hallmarks of NASH (Figure 7K). We found that the proportion of patients with HCC presenting cirrhotic lesions was significantly increased in *ADORA2A*-low versus -high subgroups (Figure 7G; 48% versus 29%, $p < 0.05$). Interestingly, we also found that the predictive value of reduced *ADORA2A* expression was restricted to patients with HCC with moderate to severe fibrosis (Figures 7H and 7I). Finally, in support of our

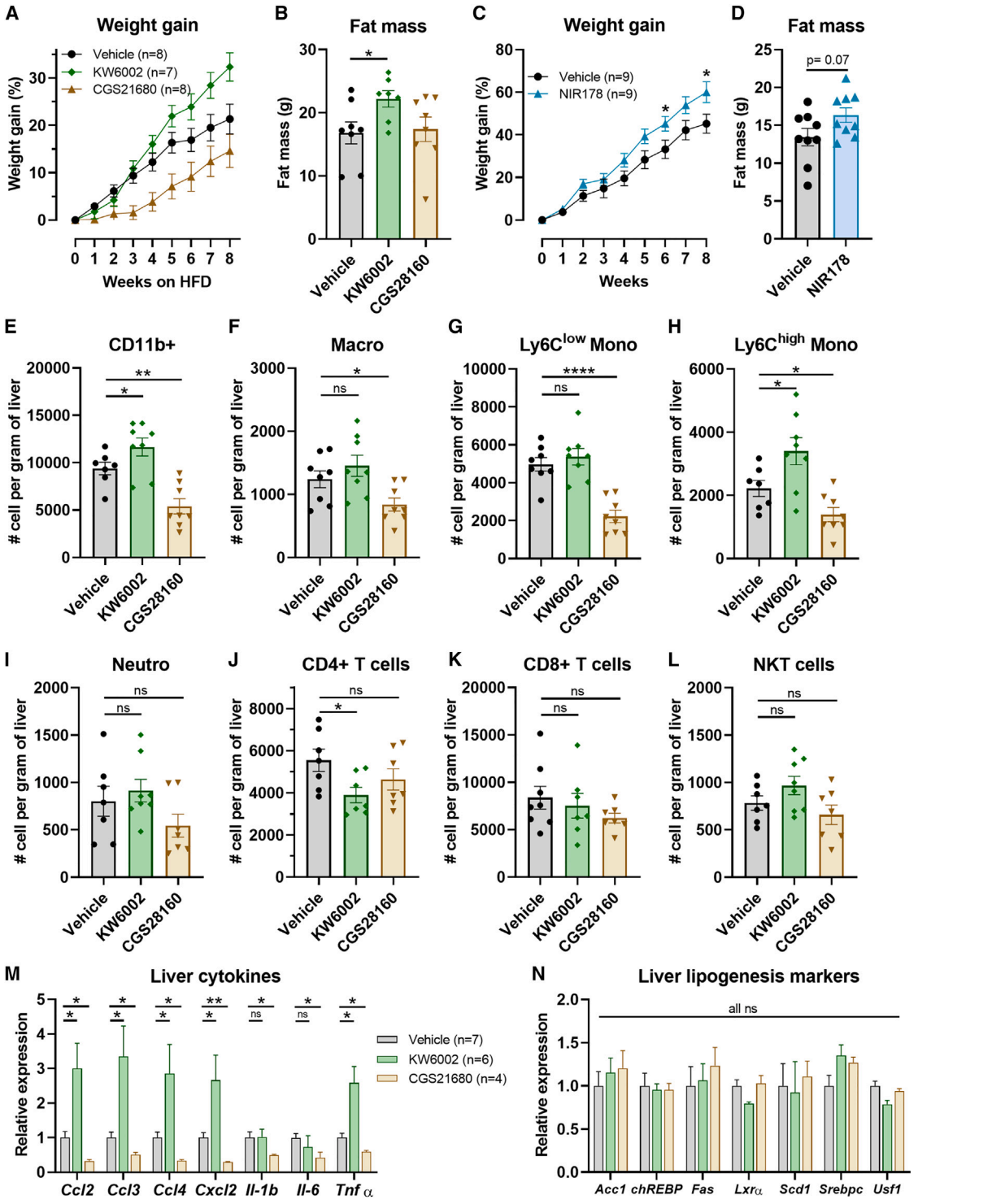

Figure 5. Pharmacological blockade of A2AR signaling promotes HFD-induced obesity and myeloid-derived liver inflammation

(A) Growth curve. WT male mice were fed with a CD-HFD and treated daily with KW6002 (10 mg/kg p.o.), CGS21680 (0.5 mg/kg i.p.), or vehicle for a total of 8 weeks. Mice weight was monitored every week.

(B) After 8 weeks of treatment, fat mass was measured using an EchoMRI.

(C) Growth curve of male C57BL/6 mice fed with a CD-HFD and treated daily with NIR178 (10 mg/kg p.o.) or vehicle.

(D) Fat mass measurement after 8 weeks of treatment with NIR178 using an EchoMRI.

(legend continued on next page)

observations in A2AR-deficient mice, we observed a higher incidence of grade 2 hepatic inflammation in patients with *ADORA2A*-low versus -high HCC (Figure 7J; 16.1% versus 3%, $p < 0.05$). Together, these results are consistent with our observations in A2AR-deficient mice and with the notion that disruption of A2AR signaling can accelerate liver carcinogenesis by promoting inflammation and fibrosis.

DISCUSSION

Incidence of HCC has substantially increased over the past two decades, making it the fourth leading cause of cancer-related deaths worldwide.[30,31] While a significant proportion of HCC can be linked to chronic viral infections and/or exposure to environmental toxins (i.e., alcohol or aflatoxin), western diet, and a sedentary lifestyle promoting obesity, NAFLD and NASH is becoming a primary cause of HCC.[32] In this study, we uncovered a critical protective role for A2AR adenosine signaling in NASH-associated HCC in mice. As numerous A2AR antagonists are currently being tested in patients with cancer, our findings have important implications in future study design and patient selection.

The impact of eADO and A2AR signaling in the TME has been extensively studied.[1] The current dogma proposes that eADO production and A2AR stimulation is a broadly immunosuppressive mechanism that favors tumor progression. Several groups, including ours, have shown that targeting A2AR or upstream ecto-nucleotidases can delay tumor growth and metastasis in multiple preclinical models and can potentiate the efficacy of other cancer immunotherapies, including PD-1/L1 checkpoint inhibitors.[4,6,9,11,14,16,33] In murine models of liver cancer, reduced tumor growth was observed upon targeted blockade of A2AR, CD73, CD39, or A2BR. Co-blockade of A2AR and CD73 displayed superior anti-tumor activity compared to single agents alone in orthotopic HCC xenograft[34]; CD39 inhibition restored sensitivity to anti-PD1 therapy in a syngeneic orthotopic HCC model[35] and reduced experimental hepatic metastases[36]; and A2BR blockade improved the anti-tumor efficacy of the VEGFR inhibitor sorafenib in the Hepa1-6 model.[37] Collectively, while all these studies support the usage of adenosine pathway inhibitors for the treatment of HCC, it remains unknown whether A2AR antagonists or other adenosine-blocking agents are also effective in the context of NASH-HCC.

A recent study by Pfister et al. supports the notion that systemic immune-stimulating therapies, including immune checkpoint blockade, can be detrimental in NASH-HCC by exacerbating $CD8^+$ T cell-mediated liver inflammation and damage instead of promoting tumor immunosurveillance.[38] Blocking A2AR signaling has also been shown to exacerbate inflammation, steatosis, and liver damage in mice fed with NASH-inducing diets.[19–23] Moreover, perturbation of liver-derived purinergic signaling in CD39 knockout mice, Entpd5 null mice, or hepatocyte-specific CD73-deficient mice led to spontaneous development of HCC[39,40] and NASH[41] in older animals. Loss of CD39 in the liver was associated with the accumulation of extracellular ATP and overactivation of the MAPK/Akt/mTOR pathway in hepatocytes leading to malignant transformation.[39] In contrast, it was proposed that lack of eADO and adenosine receptor signaling in CD73-deficient hepatocytes induces hypoactivation of the AMP-activated protein kinase (AMPK) signaling pathway leading to hepatocellular injury.[41]

In line with these findings, our study uncovered that genetic disruption of A2AR signaling spontaneously triggers systemic metabolic perturbations and promotes the development of liver steatosis, NASH, and HCC. One of the most striking observations of our study is the spontaneous development of obesity, NASH, and ultimately HCC in male A2AR-deficient mice on C57BL/6 background. Several strains of A2A knockout (A2AKO) mice have been used and studied in various laboratories[27,42,43]; however, spontaneous development of obesity upon regular chow diet feeding was not systematically reported or investigated.[19,20,27,42,44,45] For instance, Ledent et al., who initially described the phenotype of A2AR-deficient mice, mentioned an increased body mass in A2AKO animals (generated on a CD1 background) affecting both males and females.[42] Similarly, Sitkovsky and colleagues observed an increased accumulation of epididymal fat in C57BL/6 A2AR-deficient mice compared with WT animals fed with a regular chow diet (patent #WO2012027695A1). Contrasting with our results, the group of Wu and colleagues did not observe spontaneous weight gain in mice with a global deficiency in A2AR on a C57BL/6 background.[19,20,46] Exacerbated weight gain and increased severity of NAFLD and NASH in A2AR-deficient animals was, however, observed upon HFD feeding,[19] which supports our observations. To our knowledge, spontaneous development or increased susceptibility to carcinogen-induced HCC in A2AR-deficient mice has not been documented.

Exacerbated development of HCC in A2AR-deficient mice was abrogated by neutralizing key pro-inflammatory cytokines, highlighting the critical role of A2AR-mediated anti-inflammatory functions to restrain liver carcinogenesis. Importantly, we demonstrated a pivotal tumor-suppressive role for myeloid-derived A2AR in NASH-HCC development. Given that macrophage-derived TNF-α is critical for the development of NASH-associated HCC,[47] it is likely that A2AR restrains HCC progression, at least in part, by suppressing TNF-α secretion by macrophages.[48] Anti-inflammatory A2AR signaling on other immune cells also involved in NASH-HCC, such as T cells[38] and natural killer T (NKT) cells,[49] may further contribute to its

(E–L) Livers of CD-HFD-fed mice treated with KW6002, CGS21608, or vehicle were collected, and immune infiltrate was analyzed by flow cytometry: (E) CD11b+ myeloid cells, (F) CD11b+ F4/80+ macrophages, (G) CD11b+ Ly6G-$Ly6C^{low}$ monocytes, (H) CD11b+ Ly6G- $Ly6C^{high}$ inflammatory monocytes, (I) CD11b+ Ly6G+ neutrophils, (J) TCRb+ CD4+ T cells, (K) TCRb+ CD8+ T cells, and (L) TCRb+ CD11b+ NKT cells.

(M and N) Real-time PCR showing mRNA level of liver-derived cytokines and lipogenesis markers from treated mice.

Results are representative of 1 biological replicate, and sample size is indicated for each panel. Data are presented as means ± SEM. Statistical tests: Student's t test (C and D) or multiple t tests with Benjamin-Hochberg correction (A, B, and E–N).

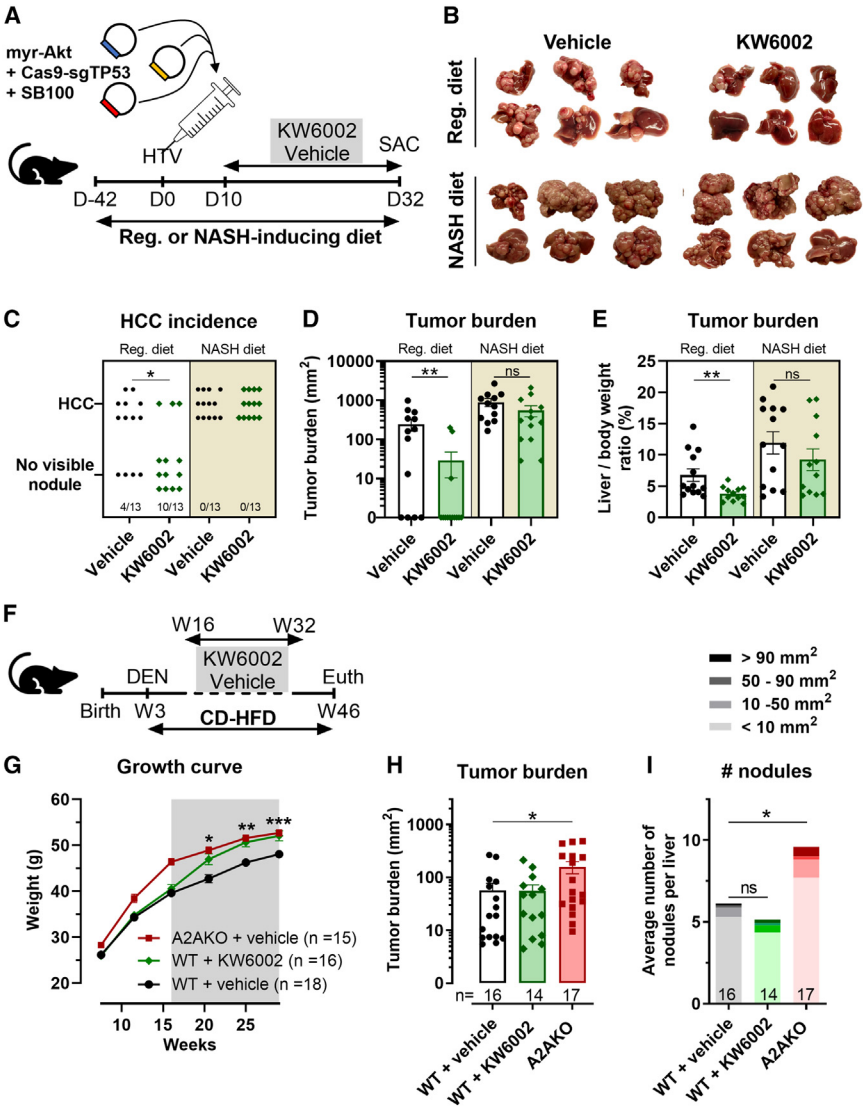

Figure 6. Diet-induced steatohepatitis impairs the anti-HCC activity of A2AR inhibition

(A) Experimental design of the hydrodynamic tail-vein HCC model.

(B) Representative pictures of livers collected on mice treated with KW6002 or vehicle subjected to regular chow diet or CD-HFD feeding.

(C) Tumor incidence as determined by visualization of macroscopic nodule on livers.

(D) Total tumor burden on livers.

(E) Liver-to-body weight ratio as a surrogate of total tumor burden.

(F) Experimental design: male WT or A2AKO animals were exposed to DEN (50 mg/kg i.p.) at 3 weeks old and fed with a CD-HFD until sacrifice. From weeks 16 to 32, mice were treated daily with KW6002 (10 mg/kg p.o.) or vehicle as indicated.

(G) Growth curve of the different group of mice.

(H) Total liver tumor burden at sacrifice.

(I) Number and size of macroscopic HCC nodules. Results are representative of 1 biological replicate, and sample size is indicated for each panel. Data are presented as means ± SEM. Statistical tests: chi-squared test (C), Mann-Whitney (D, E, H, and I), or Student's t tests (D).

tumor-suppressive function. We document a tumor-suppressor function of hepatocyte-derived A2AR signaling in a model of DMBA/CD-HFD-induced HCC. Hepatocyte-specific A2AR deficiency also promoted CD-HFD-induced obesity and the upregulation of liver-derived stearoyl-CoA desaturase-1 (Scd1) mRNA levels, a key enzyme involved in *de novo* lipogenesis that has been associated with obesity, insulin resistance, and HCC development in mice and humans.[50,51]

We demonstrated that pharmacological blockade of A2AR similarly exacerbated HFD-induced obesity and myeloid-derived liver inflammation. Indeed, treatment of HFD-fed mice with KW6002 significantly increased the number of liver-derived inflammatory monocytes and cognate pro-inflammatory/tumorigenic cytokines while simultaneously reducing the number of $CD4^+$ T cells, known to have a prominent role in NASH-HCC immunosurveillance.[52,53] In the absence of pre-existing NASH, however, KW6002 significantly suppressed HCC tumor development. This suggested that liver steatosis may influence the impact of anti-A2AR therapy on HCC. Accordingly, KW6002 lost anti-tumor activity in mice fed with a CD-HFD to induce liver steatohepatitis and mimic NASH-HCC. In the NASH-HCC microenvironment, it is conceivable that the concomitant alleviation of A2AR-mediated immunosuppressive functions on myeloid cells, coupled with impaired T cell maintenance and effector/memory differentiation, may overcome the beneficial anti-tumor effects of A2AR inhibition that were observed in HCC models not involving hepatic steatohepatitis. While A2AR inhibition with KW6002 did not accelerate NASH-HCC development, other compounds with more potent and unsurmountable antagonistic activity may promote NASH-HCC, as observed with gene-targeted mice.

Several small-molecule antagonists targeting A2AR signaling are now being evaluated in clinical trials in patients with cancer. In light of our findings, particular attention should be given to the toxicity profile of A2AR inhibitors when used in patients with pre-existing metabolic conditions, such as obesity, NAFLD, NASH, or diabetes. Notably, NASH has been shown to limit anti-tumor surveillance in immunotherapy-treated HCC.[38,53] In certain microenvironments (i.e., the fatty liver), cancer immunotherapy might even aggravate tumor progression.[38] In this context, our study may have implications for patients with cancer with NASH-HCC that receive an A2AR antagonist.

In conclusion, while targeted blockade of A2AR is intended to relieve anti-tumor immunity from adenosine-mediated immune suppression and to limit tumor development, our findings

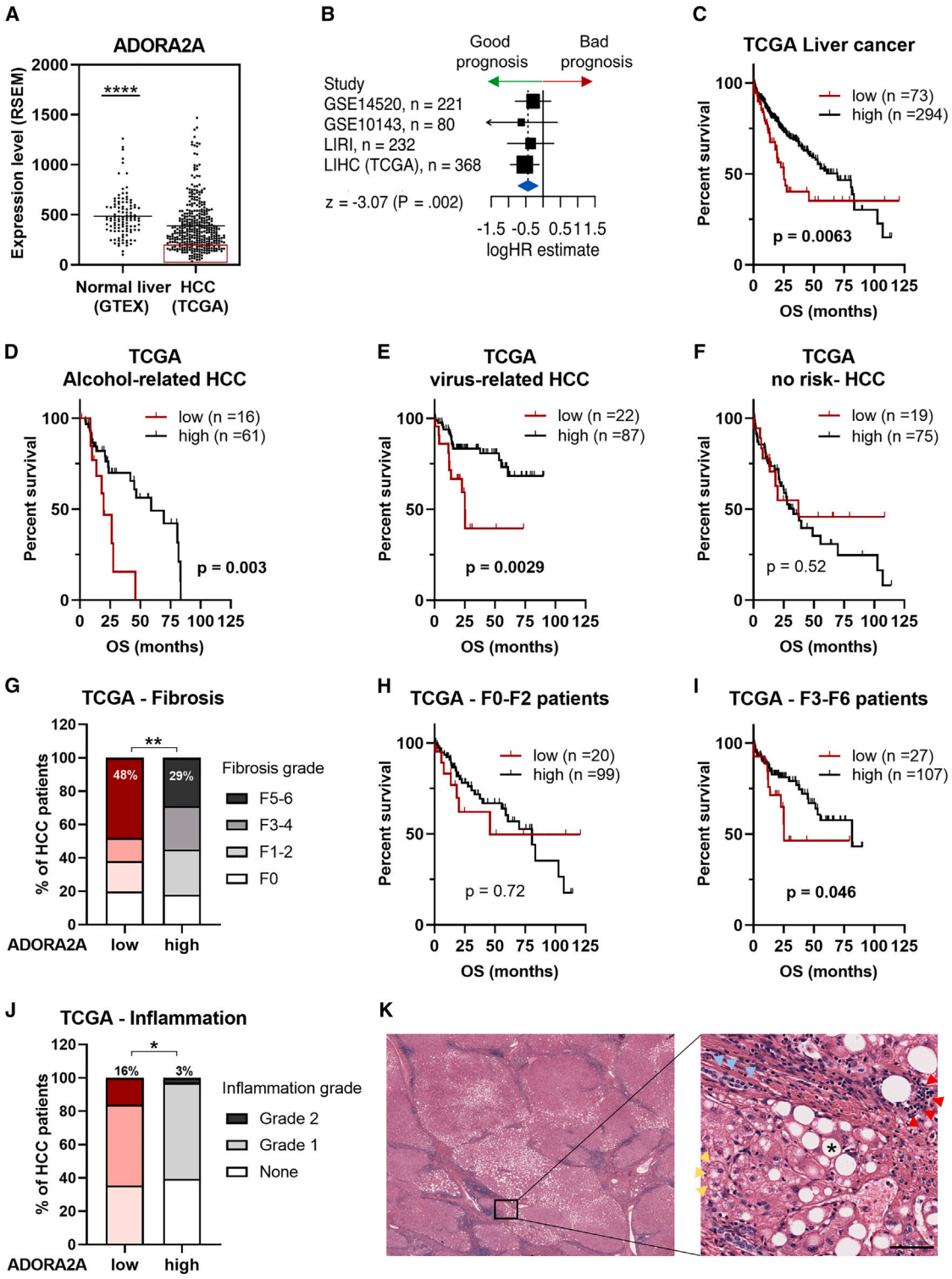

Figure 7. Reduced *ADORA2A* expression is associated with poor prognosis in patients with HCC

(A) Comparative expression of *ADORA2A* (RNA sequencing [RNA-seq] data: UCSC Xena platform) in healthy liver (GTEX) and HCC (TCGA LIHC cohort). The blue box shows the bottom 20% of patients with HCC that have low expression of *ADORA2A*.

(B) Forest plot displaying log hazard ratios (logHRs) for *ADORA2A* association with OS, using a univariate cox proportional hazards regression model. Patients were stratified into "high" and "low" subgroups using the bottom quintile of *ADORA2A* expression. Statistical significance was set at a false discovery rate (FDR)

(legend continued on next page)

highlight that this concept may not be applicable to every cancer type. In the liver, the immunosuppressive, anti-steatotic, and cytoprotective functions of A2AR signaling restrain NASH-associated HCC, which advocates caution in the clinical use of A2AR antagonists in patients with NAFLD, NASH, or NASH-HCC.

Limitations of the study

In this study, we demonstrate that A2AR signaling on immune cells and hepatocytes maintains liver immune and metabolic homeostasis to protect hepatic tissue against the development of NAFLD and its progression toward NASH and HCC. While our results clearly demonstrate the involvement of A2AR-mediated pro-inflammatory cytokine suppression and of macrophage-derived A2AR signaling to restrain liver inflammation and carcinogen-induced HCC, it remains unclear whether other A2AR-expressing immune cells may also contribute to the tumor-suppressive function of A2AR in the liver. Of note, in *lyzM-Cre*$^{+/-}$ A2AR$^{flox/flox}$ mice, while A2AR expression is efficiently silenced on macrophages, it is also most likely downregulated in other myeloid subsets such as monocytes, neutrophils, or dendritic cells,[54] which may have contributed to the phenotypes observed in our experiments. In addition, given the pivotal immunosuppressive role A2AR signaling on T cells, NK cells, or NKT cells, further experiments should be performed to clarify the involvement of those cells in the tumor-suppressive function of A2AR in the liver.

The potential mechanisms by which hepatocyte-derived A2AR signaling protects against HFD-induced obesity and restrains carcinogen-induced HCC remains to be fully characterized. We observed that hepatocyte-specific deficiency in A2AR signaling upregulates liver-derived *Scd1* mRNA levels. Whether A2AR signaling directly regulates *Scd1* expression in hepatocytes and whether this enzyme is critically involved in the development of obesity, NASH, and HCC in A2AR-deficient mice warrants further investigation.

In contrast to A2AR gene-targeted mice, we did not observe exacerbated HCC progression by blocking A2AR with chronic istradefylline treatment. Instead, we observed that blocking A2AR restrains liver tumor growth in a transposon-based, Akt/p53-driven HCC model and that this anti-HCC activity is abrogated by pre-existing NASH. Whether similar results can be obtained with other A2AR antagonists and in other types of HCC models remains to be determined. In addition, given the observations of Pfister et al.,[38] it would be of interest to test whether the combined inhibition of A2AR and PD1 further aggravates NASH-HCC as compared to anti-PD1 monotherapy. Such results, as well as a better understanding of the mechanisms by which NASH impairs the anti-tumor activity of A2AR antagonists, could help with selecting patients with HCC most susceptible to respond to anti-A2AR therapy.

Finally, the translational relevance of our finding needs to be consolidated in additional human HCC and NASH-HCC cohorts and validated at the protein level.

STAR★METHODS

Detailed methods are provided in the online version of this paper and include the following:

- KEY RESOURCES TABLE
- RESOURCE AVAILABILITY
  - Lead contact
  - Materials availability
  - Data and code availability
- EXPERIMENTAL MODEL AND STUDY PARTICIPANT DETAILS
  - Cell lines
  - Mice strains and breeding
  - Human subjects
- METHOD DETAILS
  - Carcinogen-induced liver cancer models
  - Hydrodynamic tail-vein HCC model
  - Bone marrow transplantation
  - Cytokine neutralization *in vivo*
  - Chronic treatment with A2AR antagonists and agonist *in vivo*
  - Metabolic studies
  - Histology
  - Immunofluorescence of liver samples
  - Measurement of cytokine levels in blood
  - Real-time PCR
  - Flow cytometry
  - Bioinformatic analyses
- QUANTIFICATION AND STATISTICAL ANALYSIS
  - Statistical analyses

SUPPLEMENTAL INFORMATION

Supplemental information can be found online at https://doi.org/10.1016/j.xcrm.2023.101188.

ACKNOWLEDGMENTS

We thank the CRCHUM metabolic platform for performing AlphaLISA and the CHUM clinical biochemistry platform (Dr. Sacha Obelia) for his assistance to

of 0.05 (dotted horizontal line). Horizontal bars represent the 95% confidence intervals of logHRs. The blue diamond represents the overall effect of *ADORA2A* expression in patients with HCC. The *Z* score of the overall effect corresponds to the logHR/standard error of the meta-analysis.
(C–F, H, and I) Kaplan-Meier curves showing the prognostic impact of ADORA2A expression in the TCGA HCC cohort, incorporating all patients (C) or patients with alcohol-related HCC (D), virus-related HCC (E), or HCC with no history of primary risk factors (F). In (H) and (I), the prognostic impact of *ADORA2A* expression was evaluated according to fibrosis severity. Patients were split into *ADORA2A*-low and -high groups using the bottom quintile of its expression.
(G and J) Bar graph comparing fibrosis (G) or inflammation (J) severity in patients with HCC from the TCGA cohort when stratified according to *ADORA2A* expression; ADORA2A-low and -high patients correspond to the 100 lowest and highest expressors, respectively.
(K) Diagnosis slide from an *ADORA2A*-low HCC patient (TCGA-LIHC) showing bridging fibrosis with the formation of cirrhotic liver nodule. At higher magnification, the picture shows macrovesicular steatosis (*), ballooned hepatocytes (yellow arrowheads), inflammatory cell foci (red arrowheads), and fibrosis (blue arrowheads). Scale bar represents 100 μm.
Statistical tests: Student's t test (A), log-rank rank (C–F, H, and I), or chi-squared test (G and J).

get our murine plasma samples analyzed. We are thankful to Dr. Sylvia C. Sookoian and Dr. Carlos G. Pirola for helpful discussions about this study. J.S. received a Project Grant from the Canadian Institutes of Health Research (CIHR). J.S. received a salary award from the CIHR and support from the Jean-Guy Sabourin Research Chair in Pharmacology. B.A. received postdoctoral scholarships from Mitacs, the Montreal Cancer Institute, and the Fonds de Recherche du Québec - Santé (FRQS) Institute of Cancer Research.

AUTHOR CONTRIBUTIONS

B.A. and J.S. designed the study. B.A. designed and performed most of the experiments. B.A. analyzed the data, made the figures, and wrote the manuscript. J.S. supervised the study, revised the manuscript, and raised funding. I.C., P.C., D.A., L.B., C.J.-F., and S.P. performed experiments or provided technical assistance with some experiments. Y.B. performed bioinformatic analyses. S.D. and F.A.-P. analyzed and scored liver tissue slides (NAS score, mouse liver tumor stage, and TCGA-LIHC diagnosis slide scoring). F.P. performed and analyzed the results of cardiac echography.

DECLARATION OF INTERESTS

J.S. is a paid consultant, SAB member, and owns stocks in Surface Oncology and received sponsored research grants from Surface Oncology.

INCLUSION AND DIVERSITY

We support inclusive, diverse, and equitable conduct of research.

Received: December 1, 2022
Revised: June 22, 2023
Accepted: August 15, 2023
Published: September 7, 2023

REFERENCES

1. Allard, B., Allard, D., Buisseret, L., and Stagg, J. (2020). The adenosine pathway in immuno-oncology. Nat. Rev. Clin. Oncol. *17*, 611–629. https://doi.org/10.1038/s41571-020-0382-2.
2. Fredholm, B.B. (2007). Adenosine, an endogenous distress signal, modulates tissue damage and repair. Cell Death Differ. *14*, 1315–1323. https://doi.org/10.1038/sj.cdd.4402132.
3. Ohta, A., and Sitkovsky, M. (2001). Role of G-protein-coupled adenosine receptors in downregulation of inflammation and protection from tissue damage. Nature *414*, 916–920. https://doi.org/10.1038/414916a.
4. Ohta, A., Gorelik, E., Prasad, S.J., Ronchese, F., Lukashev, D., Wong, M.K.K., Huang, X., Caldwell, S., Liu, K., Smith, P., et al. (2006). A2A adenosine receptor protects tumors from antitumor T cells. Proc. Natl. Acad. Sci. USA *103*, 13132–13137. https://doi.org/10.1073/pnas.0605251103.
5. Beavis, P.A., Divisekera, U., Paget, C., Chow, M.T., John, L.B., Devaud, C., Dwyer, K., Stagg, J., Smyth, M.J., and Darcy, P.K. (2013). Blockade of A2A receptors potently suppresses the metastasis of CD73+ tumors. Proc. Natl. Acad. Sci. USA *110*, 14711–14716. https://doi.org/10.1073/pnas.1308209110.
6. Young, A., Ngiow, S.F., Gao, Y., Patch, A.-M., Barkauskas, D.S., Messaoudene, M., Lin, G., Coudert, J.D., Stannard, K.A., Zitvogel, L., et al. (2018). A2AR Adenosine Signaling Suppresses Natural Killer Cell Maturation in the Tumor Microenvironment. Cancer Res. *78*, 1003–1016. https://doi.org/10.1158/0008-5472.CAN-17-2826.
7. Cekic, C., Day, Y.-J., Sag, D., and Linden, J. (2014). Myeloid Expression of Adenosine A2A Receptor Suppresses T and NK Cell Responses in the Solid Tumor Microenvironment. Cancer Res. *74*, 7250–7259. https://doi.org/10.1158/0008-5472.CAN-13-3583.
8. Hatfield, S.M., Kjaergaard, J., Lukashev, D., Schreiber, T.H., Belikoff, B., Abbott, R., Sethumadhavan, S., Philbrook, P., Ko, K., Cannici, R., et al. (2015). Immunological mechanisms of the antitumor effects of supplemental oxygenation. Sci. Transl. Med. *7*, 277ra30. https://doi.org/10.1126/scitranslmed.aaa1260.
9. Beavis, P.A., Milenkovski, N., Henderson, M.A., John, L.B., Allard, B., Loi, S., Kershaw, M.H., Stagg, J., and Darcy, P.K. (2015). Adenosine Receptor 2A Blockade Increases the Efficacy of Anti–PD-1 through Enhanced Antitumor T-cell Responses. Cancer Immunol. Res. *3*, 506–517. https://doi.org/10.1158/2326-6066.CIR-14-0211.
10. Beavis, P.A., Henderson, M.A., Giuffrida, L., Mills, J.K., Sek, K., Cross, R.S., Davenport, A.J., John, L.B., Mardiana, S., Slaney, C.Y., et al. (2017). Targeting the adenosine 2A receptor enhances chimeric antigen receptor T cell efficacy. J. Clin. Invest. *127*, 929–941. https://doi.org/10.1172/JCI89455.
11. Mittal, D., Young, A., Stannard, K., Yong, M., Teng, M.W.L., Allard, B., Stagg, J., and Smyth, M.J. (2014). Antimetastatic Effects of Blocking PD-1 and the Adenosine A2A Receptor. Cancer Res. *74*, 3652–3658. https://doi.org/10.1158/0008-5472.CAN-14-0957.
12. Young, A., Ngiow, S.F., Barkauskas, D.S., Sult, E., Hay, C., Blake, S.J., Huang, Q., Liu, J., Takeda, K., Teng, M.W.L., et al. (2016). Co-inhibition of CD73 and A2AR Adenosine Signaling Improves Anti-tumor Immune Responses. Cancer Cell *30*, 391–403. https://doi.org/10.1016/j.ccell.2016.06.025.
13. Loi, S., Pommey, S., Haibe-Kains, B., Beavis, P.A., Darcy, P.K., Smyth, M.J., and Stagg, J. (2013). CD73 promotes anthracycline resistance and poor prognosis in triple negative breast cancer. Proc. Natl. Acad. Sci. USA *110*, 11091–11096. https://doi.org/10.1073/pnas.1222251110.
14. Leone, R.D., Sun, I.-M., Oh, M.-H., Sun, I.-H., Wen, J., Englert, J., and Powell, J.D. (2018). Inhibition of the adenosine A2a receptor modulates expression of T cell coinhibitory receptors and improves effector function for enhanced checkpoint blockade and ACT in murine cancer models. Cancer Immunol. Immunother. *67*, 1271–1284. https://doi.org/10.1007/s00262-018-2186-0.
15. Willingham, S.B., Ho, P.Y., Hotson, A., Hill, C., Piccione, E.C., Hsieh, J., Liu, L., Buggy, J.J., McCaffery, I., and Miller, R.A. (2018). A2AR Antagonism with CPI-444 Induces Antitumor Responses and Augments Efficacy to Anti–PD-(L)1 and Anti–CTLA-4 in Preclinical Models. Cancer Immunol. Res. *6*, 1136–1149. https://doi.org/10.1158/2326-6066.CIR-18-0056.
16. Waickman, A.T., Alme, A., Senaldi, L., Zarek, P.E., Horton, M., and Powell, J.D. (2012). Enhancement of tumor immunotherapy by deletion of the A2A adenosine receptor. Cancer Immunol. Immunother. *61*, 917–926. https://doi.org/10.1007/s00262-011-1155-7.
17. Buisseret, L., Rottey, S., de Bono, J., Mossakowski, M., Delafontaine, B., Manickavasagar, T., Kotecki, N., Martinoli, C., Schneider, M., De Henau, O., et al. (2020). Abstract CT152: First in human study with EOS100850, a novel potent A2A antagonist, shows excellent tolerance and clinical benefit in immune resistant advanced cancers. Cancer Res. *80*, CT152. https://doi.org/10.1158/1538-7445.AM2020-CT152.
18. Fong, L., Hotson, A., Powderly, J.D., Sznol, M., Heist, R.S., Choueiri, T.K., George, S., Hughes, B.G.M., Hellmann, M.D., Shepard, D.R., et al. (2020). Adenosine 2A Receptor Blockade as an Immunotherapy for Treatment-Refractory Renal Cell Cancer. Cancer Discov. *10*, 40–53. https://doi.org/10.1158/2159-8290.CD-19-0980.
19. Cai, Y., Li, H., Liu, M., Pei, Y., Zheng, J., Zhou, J., Luo, X., Huang, W., Ma, L., Yang, Q., et al. (2018). Disruption of adenosine 2A receptor exacerbates NAFLD through increasing inflammatory responses and SREBP1c activity. Hepatology *68*, 48–61. https://doi.org/10.1002/hep.29777.
20. Zhou, J., Li, H., Cai, Y., Ma, L., Matthews, D., Lu, B., Zhu, B., Chen, Y., Qian, X., Xiao, X., et al. (2019). Mice lacking adenosine 2A receptor reveal increased severity of MCD-induced NASH. J. Endocrinol. *243*, 199–209. https://doi.org/10.1530/JOE-19-0198.
21. Imarisio, C., Alchera, E., Sutti, S., Valente, G., Boccafoschi, F., Albano, E., and Carini, R. (2012). Adenosine A2a Receptor Stimulation Prevents Hepatocyte Lipotoxicity and Non-alcoholic Steatohepatitis (NASH) in Rats.

Clin. Sci. (London, England : 1979) *123*, 323–332. https://doi.org/10.1042/CS20110504.

22. Alchera, E., Rolla, S., Imarisio, C., Bardina, V., Valente, G., Novelli, F., and Carini, R. (2017). Adenosine A2a receptor stimulation blocks development of nonalcoholic steatohepatitis in mice by multilevel inhibition of signals that cause immunolipotoxicity. Transl. Res. *182*, 75–87. https://doi.org/10.1016/j.trsl.2016.11.009.
23. Alchera, E., Chandrashekar, B.R., Clemente, N., Borroni, E., Boldorini, R., and Carini, R. (2021). Ischemia/Reperfusion Injury of Fatty Liver Is Protected by A2AR and Exacerbated by A1R Stimulation through Opposite Effects on ASK1 Activation. Cells *10*, 3171. https://doi.org/10.3390/cells10113171.
24. Lappas, C.M., Day, Y.-J., Marshall, M.A., Engelhard, V.H., and Linden, J. (2006). Adenosine A2A receptor activation reduces hepatic ischemia reperfusion injury by inhibiting CD1d-dependent NKT cell activation. J. Exp. Med. *203*, 2639–2648. https://doi.org/10.1084/jem.20061097.
25. Day, Y.-J., Li, Y., Rieger, J.M., Ramos, S.I., Okusa, M.D., and Linden, J. (2005). A2A Adenosine Receptors on Bone Marrow-Derived Cells Protect Liver from Ischemia-Reperfusion Injury. J. Immunol. *174*, 5040–5046. https://doi.org/10.4049/jimmunol.174.8.5040.
26. Odashima, M., Otaka, M., Jin, M., Komatsu, K., Wada, I., Matsuhashi, T., Horikawa, Y., Hatakeyama, N., Oyake, J., Ohba, R., et al. (2005). Selective A2A adenosine agonist ATL-146e attenuates acute lethal liver injury in mice. J. Gastroenterol. *40*, 526–529. https://doi.org/10.1007/s00535-005-1609-9.
27. Gnad, T., Scheibler, S., von Kügelgen, I., Scheele, C., Kilić, A., Glöde, A., Hoffmann, L.S., Reverte-Salisa, L., Horn, P., Mutlu, S., et al. (2014). Adenosine activates brown adipose tissue and recruits beige adipocytes via A 2A receptors. Nature *516*, 395–399. https://doi.org/10.1038/nature13816.
28. Anstee, Q.M., Reeves, H.L., Kotsiliti, E., Govaere, O., and Heikenwalder, M. (2019). From NASH to HCC: current concepts and future challenges. Nat. Rev. Gastroenterol. Hepatol. *16*, 411–428. https://doi.org/10.1038/s41575-019-0145-7.
29. Esser, N., Legrand-Poels, S., Piette, J., Scheen, A.J., and Paquot, N. (2014). Inflammation as a link between obesity, metabolic syndrome and type 2 diabetes. Diabetes Res. Clin. Pract. *105*, 141–150. https://doi.org/10.1016/j.diabres.2014.04.006.
30. Bray, F., Ferlay, J., Soerjomataram, I., Siegel, R.L., Torre, L.A., and Jemal, A. (2018). Global cancer statistics 2018: GLOBOCAN estimates of incidence and mortality worldwide for 36 cancers in 185 countries. CA. Cancer J. Clin. *68*, 394–424. https://doi.org/10.3322/caac.21492.
31. Ryerson, A.B., Eheman, C.R., Altekruse, S.F., Ward, J.W., Jemal, A., Sherman, R.L., Henley, S.J., Holtzman, D., Lake, A., Noone, A.-M., et al. (2016). Annual Report to the Nation on the Status of Cancer, 1975–2012, Featuring the Increasing Incidence of Liver Cancer. Cancer *122*, 1312–1337. https://doi.org/10.1002/cncr.29936.
32. El-Serag, H.B., and Kanwal, F. (2014). Epidemiology of Hepatocellular Carcinoma in the United States: Where Are We? Where Do We Go? Hepatology *60*, 1767–1775. https://doi.org/10.1002/hep.27222.
33. Giuffrida, L., Sek, K., Henderson, M.A., Lai, J., Chen, A.X.Y., Meyran, D., Todd, K.L., Petley, E.V., Mardiana, S., Mølck, C., et al. (2021). CRISPR/Cas9 mediated deletion of the adenosine A2A receptor enhances CAR T cell efficacy. Nat. Commun. *12*, 3236. https://doi.org/10.1038/s41467-021-23331-5.
34. Ma, X.-L., Shen, M.-N., Hu, B., Wang, B.-L., Yang, W.-J., Lv, L.-H., Wang, H., Zhou, Y., Jin, A.-L., Sun, Y.-F., et al. (2019). CD73 promotes hepatocellular carcinoma progression and metastasis via activating PI3K/AKT signaling by inducing Rap1-mediated membrane localization of P110β and predicts poor prognosis. J. Hematol. Oncol. *12*, 37. https://doi.org/10.1186/s13045-019-0724-7.
35. Lu, J.-C., Zhang, P.-F., Huang, X.-Y., Guo, X.-J., Gao, C., Zeng, H.-Y., Zheng, Y.-M., Wang, S.-W., Cai, J.-B., Sun, Q.-M., et al. (2021). Amplification of spatially isolated adenosine pathway by tumor–macrophage interaction induces anti-PD1 resistance in hepatocellular carcinoma. J. Hematol. Oncol. *14*, 200. https://doi.org/10.1186/s13045-021-01207-x.
36. Sun, X., Wu, Y., Gao, W., Enjyoji, K., Csizmadia, E., Müller, C.E., Murakami, T., and Robson, S.C. (2010). CD39/ENTPD1 expression by CD4+Foxp3+ regulatory T cells promotes hepatic metastatic tumor growth in mice. Gastroenterology *139*, 1030–1040. https://doi.org/10.1053/j.gastro.2010.05.007.
37. Liao, J., Zeng, D.-N., Li, J.-Z., Hua, Q.-M., Xiao, Z., He, C., Mao, K., Zhu, L.-Y., Chu, Y., Wen, W.-P., et al. (2020). Targeting adenosinergic pathway enhances the anti-tumor efficacy of sorafenib in hepatocellular carcinoma. Hepatol. Int. *14*, 80–95. https://doi.org/10.1007/s12072-019-10003-2.
38. Pfister, D., Núñez, N.G., Pinyol, R., Govaere, O., Pinter, M., Szydlowska, M., Gupta, R., Qiu, M., Deczkowska, A., Weiner, A., et al. (2021). NASH limits anti-tumour surveillance in immunotherapy-treated HCC. Nature *592*, 450–456. https://doi.org/10.1038/s41586-021-03362-0.
39. Sun, X., Han, L., Seth, P., Bian, S., Li, L., Csizmadia, E., Junger, W.G., Schmelzle, M., Usheva, A., Tapper, E.B., et al. (2013). Disordered purinergic signaling and abnormal cellular metabolism are associated with development of liver cancer in Cd39/ENTPD1 null mice. Hepatology *57*, 205–216. https://doi.org/10.1002/hep.25989.
40. Read, R., Hansen, G., Kramer, J., Finch, R., Li, L., and Vogel, P. (2009). Ectonucleoside Triphosphate Diphosphohydrolase Type 5 (Entpd5)-Deficient Mice Develop Progressive Hepatopathy, Hepatocellular Tumors, and Spermatogenic Arrest. Vet. Pathol. *46*, 491–504. https://doi.org/10.1354/vp.08-VP-0201-R-AM.
41. Alcedo, K.P., Rouse, M.A., Jung, G.S., Fu, D., Minor, M., Willcockson, H.H., Greene, K.G., and Snider, N.T. (2021). CD73 Maintains Hepatocyte Metabolic Integrity and Mouse Liver Homeostasis in a Sex-Dependent Manner. Cell. Mol. Gastroenterol. Hepatol. *12*, 141–157. https://doi.org/10.1016/j.jcmgh.2021.01.016.
42. Ledent, C., Vaugeois, J.-M., Schiffmann, S.N., Pedrazzini, T., El Yacoubi, M., Vanderhaeghen, J.-J., Costentin, J., Heath, J.K., Vassart, G., and Parmentier, M. (1997). Aggressiveness, hypoalgesia and high blood pressure in mice lacking the adenosine A 2a receptor. Nature *388*, 674–678. https://doi.org/10.1038/41771.
43. Chen, J.-F., Huang, Z., Ma, J., Zhu, J., Moratalla, R., Standaert, D., Moskowitz, M.A., Fink, J.S., and Schwarzschild, M.A. (1999). A2A Adenosine Receptor Deficiency Attenuates Brain Injury Induced by Transient Focal Ischemia in Mice. J. Neurosci. *19*, 9192–9200. https://doi.org/10.1523/JNEUROSCI.19-21-09192.1999.
44. Corciulo, C., Lendhey, M., Wilder, T., Schoen, H., Cornelissen, A.S., Chang, G., Kennedy, O.D., and Cronstein, B.N. (2017). Endogenous adenosine maintains cartilage homeostasis and exogenous adenosine inhibits osteoarthritis progression. Nat. Commun. *8*, 15019–15113. https://doi.org/10.1038/ncomms15019.
45. Csóka, B., Törő, G., Vindeirinho, J., Varga, Z.V., Koscsó, B., Németh, Z.H., Kókai, E., Antonioli, L., Suleiman, M., Marchetti, P., et al. (2017). A2A adenosine receptors control pancreatic dysfunction in high-fat-diet-induced obesity. FASEB. J. *31*, 4985–4997. https://doi.org/10.1096/fj.201700398R.
46. Pei, Y., Li, H., Cai, Y., Zhou, J., Luo, X., Ma, L., McDaniel, K., Zeng, T., Chen, Y., Qian, X., et al. (2018). Regulation of Adipose Tissue Inflammation by Adenosine 2A Receptor in Obese Mice. J. Endocrinol. *239*, 365–376. https://doi.org/10.1530/JOE-18-0169.
47. Nakagawa, H., Umemura, A., Taniguchi, K., Font-Burgada, J., Dhar, D., Ogata, H., Zhong, Z., Valasek, M.A., Seki, E., Hidalgo, J., et al. (2014). ER Stress Cooperates with Hypernutrition to Trigger TNF-Dependent Spontaneous HCC Development. Cancer Cell *26*, 331–343. https://doi.org/10.1016/j.ccr.2014.07.001.
48. Haskó, G., Kuhel, D.G., Chen, J.-F., Schwarzschild, M.A., Deitch, E.A., Mabley, J.G., Marton, A., and Szabó, C. (2000). Adenosine inhibits IL-12 and TNF-α production via adenosine A2a receptor-dependent and independent mechanisms. FASEB J *14*, 2065–2074. https://doi.org/10.1096/fj.99-0508com.

49. Wolf, M.J., Adili, A., Piotrowitz, K., Abdullah, Z., Boege, Y., Stemmer, K., Ringelhan, M., Simonavicius, N., Egger, M., Wohlleber, D., et al. (2014). Metabolic activation of intrahepatic CD8+ T cells and NKT cells causes nonalcoholic steatohepatitis and liver cancer via cross-talk with hepatocytes. Cancer Cell *26*, 549–564. https://doi.org/10.1016/j.ccell.2014.09.003.

50. Lai, K.K.Y., Kweon, S.-M., Chi, F., Hwang, E., Kabe, Y., Higashiyama, R., Qin, L., Yan, R., Wu, R.P., Lai, K., et al. (2017). Stearoyl-CoA Desaturase Promotes Liver Fibrosis and Tumor Development in Mice via Wnt Signaling and Stabilization of Low Density Lipoprotein Receptor-related Proteins 5 and 6. Gastroenterology *152*, 1477–1491. https://doi.org/10.1053/j.gastro.2017.01.021.

51. Ntambi, J.M., Miyazaki, M., Stoehr, J.P., Lan, H., Kendziorski, C.M., Yandell, B.S., Song, Y., Cohen, P., Friedman, J.M., and Attie, A.D. (2002). Loss of stearoyl–CoA desaturase-1 function protects mice against adiposity. Proc. Natl. Acad. Sci. USA *99*, 11482–11486. https://doi.org/10.1073/pnas.132384699.

52. Ma, C., Kesarwala, A.H., Eggert, T., Medina-Echeverz, J., Kleiner, D.E., Jin, P., Stroncek, D.F., Terabe, M., Kapoor, V., ElGindi, M., et al. (2016). NAFLD causes selective CD4+ T lymphocyte loss and promotes hepatocarcinogenesis. Nature *531*, 253–257. https://doi.org/10.1038/nature16969.

53. Heinrich, B., Brown, Z.J., Diggs, L.P., Vormehr, M., Ma, C., Subramanyam, V., Rosato, U., Ruf, B., Walz, J.S., McVey, J.C., et al. (2021). Steatohepatitis Impairs T-cell-Directed Immunotherapies Against Liver Tumors in Mice. Gastroenterology *160*, 331–345.e6. https://doi.org/10.1053/j.gastro.2020.09.031.

54. Abram, C.L., Roberge, G.L., Hu, Y., and Lowell, C.A. (2014). Comparative analysis of the efficiency and specificity of myeloid-Cre deleting strains using ROSA-EYFP reporter mice. J. Immunol. Methods *408*, 89–100. https://doi.org/10.1016/j.jim.2014.05.009.

55. Bastia, E., Xu, Y.-H., Scibelli, A.C., Day, Y.-J., Linden, J., Chen, J.-F., and Schwarzschild, M.A. (2005). A Crucial Role for Forebrain Adenosine A2A Receptors in Amphetamine Sensitization. Neuropsychopharmacol *30*, 891–900. https://doi.org/10.1038/sj.npp.1300630.

56. Hernandez, C., Huebener, P., Pradere, J.-P., Antoine, D.J., Friedman, R.A., and Schwabe, R.F. (2018). HMGB1 links chronic liver injury to progenitor responses and hepatocarcinogenesis. J. Clin. Invest. *128*, 2436–2451. https://doi.org/10.1172/JCI91786.

57. Kleiner, D.E., Brunt, E.M., Van Natta, M., Behling, C., Contos, M.J., Cummings, O.W., Ferrell, L.D., Liu, Y.-C., Torbenson, M.S., Unalp-Arida, A., et al. (2005). Design and validation of a histological scoring system for nonalcoholic fatty liver disease. Hepatology *41*, 1313–1321. https://doi.org/10.1002/hep.20701.

58. Xue, W., Chen, S., Yin, H., Tammela, T., Papagiannakopoulos, T., Joshi, N.S., Cai, W., Yang, G., Bronson, R., Crowley, D.G., et al. (2014). Nature *514*, 380–384. https://doi.org/10.1038/nature13589.

59. Mates, L., Chuah, M.K.L., Belay, E., Jerchow, B., Manoj, N., Acosta-Sanchez, A., Grzela, D.P., Schmitt, A., Becker, K., Matrai, J., et al. (2009). Nat. Genet. *41*, 753–761. https://doi.org/10.1038/ng.343.

60. Yoshimoto, S., Loo, T.M., Atarashi, K., Kanda, H., Sato, S., Oyadomari, S., Iwakura, Y., Oshima, K., Morita, H., Hattori, M., et al. (2013). Obesity-induced gut microbial metabolite promotes liver cancer through senescence secretome. Nature *499*, 97–101. https://doi.org/10.1038/nature12347.

61. Xue, X., Pech, N.K., Shelley, W.C., Srour, E.F., Yoder, M.C., and Dinauer, M.C. (2010). Antibody targeting KIT as pretransplantation conditioning in immunocompetent mice. Blood *116*, 5419–5422. https://doi.org/10.1182/blood-2010-07-295949.

STAR★METHODS

KEY RESOURCES TABLE

REAGENT or RESOURCE	SOURCE	IDENTIFIER
Antibodies		
Rat anti-mouse cKit (clone ACK2)	BioXcell	Cat# BE0293, RRID:AB_2687818
Rat anti-mouse CD4 (clone GK1.5)	BioXcell	Cat# BE0003-1, RRID:AB_1107636
Rat anti-mouse CD8 (clone 53-3-8)	BioXcell	Cat# BE0223, RRID:AB_2687706
Rat anti-mouse IL-6 (clone MP5-20F3)	BioXcell	Cat# BE0046, RRID:AB_1107709
Rat anti-mouse TNF-a (clone XT3.11)	BioXcell	Cat# BE0058, RRID:AB_1107764
Mouse anti-mouse IL-17A (clone 17F3)	BioXcell	Cat# BE0173, RRID:AB_10950102
Hamster anti-mouse/rat IL-1b (clone B122)	BioXcell	Cat# BE0246, RRID:AB_2687727
Anti human/mouse A2AR (clone 7F6-G5-A2)	Novus Biologicals	Cat# NBP1-39474, RRID:AB_2226520
Rat anti-mouse F4/80 Alexa 594 (clone BM8)	Biolegend	Cat# 123140, RRID:AB_2563241
Goat Anti-mouse IgG Alexa Fluor 647	Thermo Fisher	Cat# A-21241, RRID:AB_2535810
Rat anti-mouse CD45.2 BUV 395 (clone 104)	BD Bioscience	Cat# 564616, RRID:AB_2738867
Rat anti-mouse CD45.1 FITC (clone A20)	BD Bioscience	Cat# 561871, RRID:AB_10926208
Rat anti-mouse CD11 BUV 395 (clone M1/70)	BD Bioscience	Cat# 563553, RRID:AB_2738276
Rat anti-mouse F4/80 PE (clone BM8)	Biolegend	Cat# 123110, RRID:AB_893486
Rat anti-mouse anti-TCRb FITC (clone QA18A18)	Biolegend	Cat# 159705, RRID:AB_2888830
Rat anti-mouse anti-CD4 BUV737 (clone RM4.5)	BD Bioscience	Cat# 612844, RRID:AB_2870166
Rat anti-mouse anti-CD8 BV650 (clone 53–6.7)	BD Bioscience	Cat# 563234, RRID:AB_2738084
Rat anti-mouse anti-NK1.1 Alexa 700 (clone PK136)	BD Bioscience	Cat# 560515, RRID:AB_10612564
Rat anti-mouse anti-Ly6C PerCP Cy5.5 (clone AI-21)	BD Bioscience	Cat# 560525, RRID:AB_1727558
Rat anti-mouse anti-Ly6G APC-Cy7 (clone 1A8)	BD Bioscience	Cat# 560600, RRID:AB_1727561
Bacterial and virus strains		
AAV.TBG.PI.Cre.rBG	University of Pennsylvania Vector Core	RRID:Addgene_107787
pAAV.TBG.PI.eGFP.WPRE.bGH	University of Pennsylvania Vector Core	RRID:Addgene_105535
Biological samples		
Mouse liver paraffin blocks	This paper	N/A
Chemicals, peptides, and recombinant proteins		
Dimethylbenzyl anthracene (DMBA)	Sigma	Cat# D3254-1G
Acetone	Fisher chemical	Cat# A16P-4
Diethylnitrosamine (DEN)	Sigma	Cat# N0258-1G
Carbon tetrachloride (CCl4)	Sigma	Cat# 270652-100ML
Corn Oil	Sigma	Cat# C8267-500ML
Mirus TransIT QR solution	Mirus Bio	Cat# MIR 5240
Istradefylline/KW6002	Toronto Research Chemicals	Cat# I927000
NIR178/Taminadenant	MedChem Express	Cat# HY-109139
CGS21680	Tocris	Cat# 1063
Glucose solution	Wisent	Cat# 609-035-EL
Percoll solution	Sigma	Cat# P1644-1L
Target retrieval solution	Dako	Cat# S1699
Protein block solution	Dako	Cat# X0909
(4′,6-Diamidino-2-Phenylindole, Dihydrochloride) DAPI	Thermofisher	Cat# D1306
RNA later	Thermofisher	Cat# AM7021

(*Continued on next page*)

Continued

REAGENT or RESOURCE	SOURCE	IDENTIFIER
Superscript Vilo master mix	Thermofisher	Cat# 11755050
Critical commercial assays		
Qiagen Endofree plasmid maxi kit	Qiagen	Cat# 12362
RNAeasy plus kit	Qiagen	Cat# 74034
Picrosirius red staining kit	Polysciences	Cat# 24901-250
AlphaLISA insulin kit	Perkin Elmer	Cat# AL3184C
AlphaLISA leptin kit	Perkin Elmer	Cat# AL521C
AlphaLISA TNFa kit	Perkin Elmer	Cat# L505C
U-PLEX Mouse IL-17A Assay	Meso Scale Diagnostics	Cat# K152UTK
U-PLEX Mouse TNF-α Assay	Meso Scale Diagnostics	Cat# K152UCK
U-PLEX Mouse IL-6 Assay	Meso Scale Diagnostics	Cat# K152TXK
U-PLEX Mouse KC/GRO Assay	Meso Scale Diagnostics	Cat# K152VWK
U-PLEX Mouse IL-1β Assay	Meso Scale Diagnostics	Cat# K152TUK
Mouse resisitin ELISA kit	R&D systems	Cat# DY1069
Mouse C-reactive protein ELISA kit	R&D systems	Cat# DY1829
Mouse Plaminogen activatot inhibitor ELISA kit	R&D systems	Cat# DY3828-05
Mouse adiponectin ELISA kit	R&D systems	Cat# DY1119
Deposited data		
TCGA LIHC transcriptomic data	UCSC Xena Browser	https://xenabrowser.net/datapages/
TCGA LIHC diagnostic slides	GDC portal	https://portal.gdc.cancer.gov/projects/TCGA-LIHC
Human HCC transcriptomic data	GEO portal; Roessler et al.[55]	GSE14520
Human HCC transcriptomic data	GEO portal; Hoshida et al.[56]	GSE10143
Human HCC transcriptomic data	ICGC data portal	LIRI-JP
Experimental models: Organisms/strains		
C57BL/6 *Adora2a* -/-	Chen et al.[43]	N/A
B6; 129-Adora2atm1Dyj/J	Jackson laboratories	RRID:IMSR_JAX:010687
B6.129P2-Lyz2tm1(cre)Ifo/J	Jackson laboratories	RRID:IMSR_JAX:004781
B6.SJL-Ptprca Pepcb/BoyJ	Jackson laboratories	RRID:IMSR_JAX:002014
C57BL/6J	Jackson laboratories	RRID:IMSR_JAX:000664
Oligonucleotides		
qPCR Primers, see Table S2	This paper	N/A
Recombinant DNA		
pT3-myr-AKT-HA	Calvisi et al.[57]	RRID:Addgene_31789
pX330 p53	Xue et al.[58]	RRID:Addgene_59910
pCMV(CAT)T7-SB100	Mates et al.[59]	RRID:Addgene_34879
Software and algorithms		
Visiomorph	Visiopharm	https://visiopharm.com/
ZEN Digital Imaging for Light Microscopy	Zeiss	RRID:SCR_013672
R-4.3.1	The R project	RRID:SCR_001905
Graphpad Prism	Graphpad software	RRID:SCR_002798
Other		
Choline-deficient high fat diet (CD-HFD)	Research Diets	Cat# D05010403i
Body composition analyzer	Echo MRI	Echo MRI-500
Glucometer	Aviva	Accucheck
Metabolic Cages	Columbus Instruments International	CLAMS system
Microscope slide scanner	Olympus	BX61VS. scanner
Mesoscale instrument	Mesoscale diagnostics	MESO QuickPlex SQ 120MM
Real time PCR plate reader and analyzer	Applied Biosystems	StepOne Plus

RESOURCE AVAILABILITY

Lead contact

Requests for resources, reagents and further information should be directed to and will be addressed by the lead contact, Dr. John Stagg (john.stagg@umontreal.ca).

Materials availability

All materials generated in this study will be provided upon request to the lead contact.

Data and code availability

- This paper analyzes existing, publicly available data. These accession numbers for the datasets are listed in the key resources table. All data reported in this paper will be shared by the lead contact upon request.
- This paper does not report original code.
- Any additional information required to reanalyze the data reported in this paper is available from the lead contact upon request.

EXPERIMENTAL MODEL AND STUDY PARTICIPANT DETAILS

Cell lines

This study did not use cell line.

Mice strains and breeding

All mice were maintained 5 per cages in a specific pathogen–free facility with free access to food and water, nesting material and housed at a temperature of 21°C unless otherwise stated. Most mice used for the experiments were males unless otherwise stated. A2AR-deficient mice on a C57BL/6N background were obtained from Dr. JF Chen[43] (Boston, MA) and bred at the CHUM research center. A2AR floxed mice[55] and Cre recombinase expressing mice under the control of the *Lyz2* promoter, on C57BL/6J background, were obtained from Jackson laboratory. Homozygous A2A floxed mice were crossed with LysM-Cre mice to generate myeloid cell-specific ($LysMCre^{+/-}$ $A2AR^{fl/fl}$) A2AR-deficient mice and littermate controls. To generate hepatocyte-specific A2AR-deficient mice, 3–4 weeks old homozygous A2A floxed mice were injected intravenously (retroorbital) with 1×10^{11} genome copies of AAV8-TBG-Cre adenoviruses (addgene # 107787-AAV8) driving Cre recombinase expression under the thyroglobulin promoter; control mice were injected with AAV8-TBG-eGFP adenoviruses (addgene # 105535-AAV8). All experiments were conducted with at least 5 mice per group and were reviewed and approved by the CHUM research center Animal Ethics Committee.

Human subjects

Results related to human HCC were generated using publicly available transcriptomic datasets and digital pathology images (see details in the section dedicated to bioinformatic methods below).

METHOD DETAILS

Carcinogen-induced liver cancer models

Spontaneous HCC model

WT and A2AR-deficient males were breeded under regular housing conditions and sacrificed at 80 weeks of age. Livers were collected and visually inspected for macroscopic lesions. Livers were fixed in formalin and embedded in paraffin to perform histological sections (hematoxylin/Eosin staining, picrosirius red staining) and stage tumors as described.[39]

DMBA model

DMBA (dimethylbenzyl anthracene) was used to induce the formation of liver HCC, as described by Yoshimoto et al.[60] DMBA was dissolved in acetone at a concentration of 5 mg/mL and applied topically, on the dorsal skin of 3–4 days old pups. DMBA treated mice developed macroscopic liver tumors within 40 weeks following DMBA treatment.

DEN models

A single dose of DEN (diethylnitrosamine, 50 mg/kg) was injected i.p in 3 weeks old males. Mice were sacrificed at 52 weeks of age and macroscopic liver nodules were enumerated and measured. In some experiments DEN injection was coupled to repetitive carbon tetrachloride injections (CCl_4, 15 injections from week 6–21) at a dose of 0.15 μL/gram. CCl_4 was dissolved 1:3 (volume: volume) in corn oil before injection as previously described.[56] In the DEN +CCl_4 model, mice were euthanized at 30 weeks of age to evaluate macroscopic liver nodules. In another experiment, DEN treatment was associated with feeding mice with a choline-deficient high-fat diet (CD-HFD, 65% Kcal fat, Research Diets, D05010403i). Under these experimental conditions, mice were sacrificed at 46 weeks of age to evaluate tumor burden in the liver.

Hydrodynamic tail-vein HCC model

8-10 weeks old C57BL/6J males (Jackson Lab) received 12 μg of pT3-myr-Akt-HA (Addgene #31789), 14 μg of px330-sg-p53 (Addgene #59910) and 2 μg of pCMV-SB100 (Addgene #34879) (4:1 ratio of transposon to SB100 transposase encoding plasmid) dissolved 1.8–2 mL of Mirus TransIT QR solution. Mice were injected with the solution containing the plasmid mix into the lateral tail vein with a total volume corresponding to 8% of body weight in 5–7 s. Plasmidic vectors for hydrodynamic delivery were produced using the QIAGEN Endofree plasmid Maxi kit.

Bone marrow transplantation

To minimize the impact of lethal whole-body irradiation on weight gain, a low dose irradiation protocol adapted from Xue et al.[61] was used. 3 to 4 weeks old WT and A2AKO males were treated with anti-cKit monoclonal antibody (Clone ACK2), administered i.p at a dose of 25 μg/gram, to deplete hematopoietic stem cells. 4 days after anti-cKit treatment, mice received a low dose irradiation (300 Rads) coupled to the administration of anti-CD4 (clone GK1.5) and anti-CD8 (clone 53-5-8) depleting antibodies, both at 10 mg/kg, i.p. 3 days after irradiation, mice were transplanted with 5 million bone marrow cells collected from WT CD45.1 congenic mice or A2AKO mice; at the same time, mice received a second i.p injection of anti-CD4 and anti-CD8 depleting antibodies. Engraftment rate was measured 8 weeks after transplantation.

Cytokine neutralization *in vivo*

DMBA-treated A2AKO males were treated with neutralizing monoclonal antibodies targeting IL6 (clone MP5-20F3), TNFα (clone XT3.11), IL17A (clone 17F3) or IL1β (clone B122). All antibodies were from BioXcell. Treatments started on week 20 after DMBA application and lasted until week 40. In each treatment group, mice received 250 μg of one neutralizing mAb, twice per week until the end of the experiment.

Chronic treatment with A2AR antagonists and agonist *in vivo*

8-10 weeks old C57BL/6J males (Jackson Lab) received daily administrations of KW6002 (Istradefylline, Toronto Research Chemicals), NIR178 (Taminadenant, Selleckchem) or CGS21680 (Selleckchem). KW6002 and NIR178 were administered *per os* at a dose of 10 mg/kg. KW6002 and NIR178 powders were resuspended in a solution containing 0.5% methylcellulose and 0.2% Tween 80. CGS21680 was injected i.p at a dose of 0.5 mg/kg in PBS.

Metabolic studies

Growth curves

Growth of mice (males and females) was monitored weekly by measuring weight until 32 weeks of age. In some experiments, mice were fed with a choline deficient high-fat-diet (65% Kcal fat, Research Diets, D05010403i) as detailed in figure legends. At 24 weeks of age, body composition of WT and A2AKO males was analyzed using an EchoMRI body composition analyzer. Growth monitoring of tissue-specific A2AR deficient mice and A2AR floxed mice were done only for males. At 32 weeks old, WT and A2AKO mice were sacrificed and the different subcutaneous and visceral fat deposits were collected and weighed.

Glucose tolerance test

24 weeks old WT and A2AKO males were subjected to an oral glucose tolerance test (OGTT). Mice were challenged with an oral dose of dextrose of 2 g/kg of lean mass. Blood concentrations of insulin and glucose were monitored several times over 120 min after the oral glucose challenge. Blood glucose concentrations were measured using a glucometer (Accucheck, Aviva) and insulin concentrations were determined by an AlphaLISA (PerkinElmer) following the manufacturer's protocol.

Energy expenditure measurement

Respiratory exchange ratio (RER), energy expenditure and locomotor activity were measured by indirect calorimetry in a Comprehensive Lab Animal Monitoring System metabolic cages (CLAMS, Columbus Instruments International, Columbus, OH, USA). Animals were single housed in CLAMS apparatus at 21 ± 0.2°C in a dark-light cycle during 24 h to acclimate before any measurements. Following acclimation, energy balance parameters were measured during 48h. Energy expenditure was normalized by lean mass.

Histology

Adipose tissue

Gonadal white adipose tissue (gWAT) and brown adipose tissue (BAT) deposits were embedded in paraffin to make histological slides. gWAT and BAT sections were imaged on a scanner in the Cy5 channel to take advantage of adipocyte autofluorescence. Slides of fat tissues were analyzed using the visiomorph software to determine the average adipocyte size in gWAT and BAT samples.

Liver

Livers from 32-weeks old WT and A2AKO mice were collected, fixed and embedded in paraffin to prepare histological sections. Hematoxylin and eosin staining of liver slides were analyzed and scored by a pathologist to determine a non-alcoholic steatohepatitis score (NAS) ranging from 0 to 8 as described by Kleiner et al.[57] In some experiments, liver FFPE histological slides were stained with picrosirius red staining kit (Polysciences) to reveal collagen deposits and evaluate fibrosis severity. The percentage of Sirius red positive area on each sample was quantified using the visiomorph software. Diagnostic slides from

human HCC patients were accessed from the Genomic Data Commons (GDC) data portal and reviewed by a pathologist to score inflammation, steatosis, hepatocyte ballooning and fibrosis.

Immunofluorescence of liver samples

Livers were collected, fixed and embedded in paraffin to prepare histological sections. For AAV injected mice, livers were collected 2 weeks after AAV inoculation. 5 μm sections were deparaffinized and rehydrated with xylene and alcohol, followed by antigen retrieval in citrate buffer (target retrieval solution; Dako, S1699). Protein block solution (Dako, 100%) was added for 30 min prior to an overnight incubation at 4°C with primary antibodies: anti-human/mouse A2AR mAb (clone 7F6-G5-A2, Novus biologicals) and efluor 550-coupled anti-F4/80 mAb (clone BM8, Biolegend). The following day, anti-mouse IgG2a 647 (Life technologies) was incubated for 2 h at room temperature, followed by 4′,6-diamidino-2-phenylindole (DAPI; Sigma) DNA staining and slides were mounted using ProLong Gold (ThermoFisher). Slides were then imaged using an Olympus BX61VS. slide scanner. A2AR positive areas were determined using Zen blue software (Zeiss) and normalized with the total sample area to get the percentage of A2AR positive area in each sample.

Measurement of cytokine levels in blood

Blood levels of IL17-A, Gro-α, TNF-α and IL-6 were measured using a Mesoscale multiplex assay (MSD). Blood levels of resistin, adiponectin, C-reactive protein (CRP) and plasminogen activator inhibitor 1 (PAI1) where measured using standard ELISA kits (R&D Systems). Blood levels of leptin were measured using an AlphaLISA immunoassay (PerkinElmer). All the assays were performed according to manufacturers' protocols.

Real-time PCR

Tissues were collected and placed in RNA later. RNA was extracted using RNAeasy plus kit (Qiagen) according to manufacturers' recommendations. Reverse transcription was performed using the Superscript Vilo reverse transcriptase (Life technologies). Absolute quantities of mRNA were determined with specific Taqman probes (Table S2) using a StepOne Plus real-time PCR system (Applied Biosystems).

Flow cytometry

Livers of KW6002, CGS21680 or vehicle treated mice were perfused *in situ* with 10mL of PBS, collected and manually disaggregated on a 100 μm cell strainer. Liver-infiltrating immune cells were isolated by centrifugation using a 37% Percoll gradient. Samples were then stained with a cocktail of fluorescently labeled antibodies to detect immune cell subsets. Fluorochrome labeled antibodies used in this study are listed in the key resources table. Immune cell subsets were identified as follow: Macrophages (CD45.2+/CD11b+/Ly6G-/F4/80+); Monocytes (CD45.2+/CD11b+/Ly6G-/Ly6C+/F4/80-); Neutrophils (CD45.2+/CD11b+/Ly6G+); CD4 and CD8 T cells (CD45.2+/TCRb+/$CD4^+$ or $CD8^+$); NKT cells (CD45.2+/TCRb+/CD11bdim).

Bioinformatic analyses

Clinical data and *ADORA2A* gene expression in different cohorts of HCC was collected from the UCSC Xena genomic browser (TCGA LIHC cohort), the GEO plateform (GSE14520, GSE10143) and the International Cancer Genome Consortium data portal (LIRI cohort). Comparative expression of *ADORA2A* in normal liver (GTEX) and HCC (TCGA LIHC cohort) was evaluated using the UCSC Xena TCGA-TARGET-GTEX dataset in which TCGA and GTEX mRNA have been normalized to allow comparison. In the 4 different cohorts, patients were stratified in ''high'' and ''low'' populations according to *ADORA2A* expression level: the ''low'' subgroup corresponds to the bottom 20% of *ADORA2A* expression while the ''high'' subgroup include patients with the top 80% of *ADORA2A* expression. Impact of *ADORA2A* expression on HCC patient survival was evaluated using a log rank test. For meta-analysis, forest plot displaying log hazard ratios (logHR) and 95% confidence intervals (CI) for *ADORA2A* association with OS, using a univariate cox proportional hazards regression model. *ADORA2A* expression was stratified into ''High'' and ''Low'' subgroup using the bottom 20 percent of its expression. The results of individual studies were pooled using random-effects meta-analysis with inverse variance weighting in DerSimonian and Laird random-effects models. Heterogeneity across studies was evaluated by using the Q statistic (X2) along with I2 index. All statistical analyses were performed as two-sided and p values were corrected for multiple testing using the Benjamini-Hochberg (False Discovery Rate, FDR) method. Associations were deemed statistically significant for FDR lower or equal to 0.05.

QUANTIFICATION AND STATISTICAL ANALYSIS

Statistical analyses

Unless otherwise stated, data are shown as means ± SEM. All data were analyzed using GraphPad prism software or R for bioinformatic analyses. Statistics are calculated using unpaired Student's T test or Mann-Whitney test (2 groups) or multiple T tests with Benjamin Hochberg multiple comparison correction (more than 2 groups). For some experiments, Chi2 or log-rank tests were used to compare the experimental groups as specified in figure legends. $*p < 0.05$, $**p < 0.01$, $***p < 0.001$, $****p < 0.0001$. Specific sample size are indicated in figures.